Cell Stem Cell
Article

A Mammary Stem Cell Population Identified and Characterized in Late Embryogenesis Reveals Similarities to Human Breast Cancer

Benjamin T. Spike,[1,2,4] Dannielle D. Engle,[1,3,4,5] Jennifer C. Lin,[1,4] Samantha K. Cheung,[1,6] Justin La,[1] and Geoffrey M. Wahl[1,*]
[1]Gene Expression Laboratory, Salk Institute for Biological Studies, La Jolla, CA 92037, USA
[2]Department of Chemistry and Biochemistry, University of California, San Diego, La Jolla, CA 92037, USA
[3]Division of Biological Sciences, University of California, San Diego, La Jolla, CA 92037, USA
[4]These authors contributed equally to this work
[5]Present address: Cambridge Research Institute, Cancer Research United Kingdom, Cambridge CB20RE, UK
[6]Present address: Division of Molecular and Cellular Biology, University of California, Berkeley, Berkeley, CA 94720, USA
*Correspondence: wahl@salk.edu
DOI 10.1016/j.stem.2011.12.018

SUMMARY

Gene expression signatures relating mammary stem cell populations to breast cancers have focused on adult tissue. Here, we identify, isolate, and characterize the fetal mammary stem cell (fMaSC) state since the invasive and proliferative processes of mammogenesis resemble phases of cancer progression. fMaSC frequency peaks late in embryogenesis, enabling more extensive stem cell purification than achieved with adult tissue. fMaSCs are self-renewing, multipotent, and coexpress multiple mammary lineage markers. Gene expression, transplantation, and in vitro analyses reveal putative autocrine and paracrine regulatory mechanisms, including ErbB and FGF signaling pathways impinging on fMaSC growth. Expression profiles from fMaSCs and associated stroma exhibit significant similarities to basal-like and Her2$^+$ intrinsic breast cancer subtypes. Our results reveal links between development and cancer and provide resources to identify new candidates for diagnosis, prognosis, and therapy.

INTRODUCTION

Breast cancers are a heterogeneous group of diseases distinguishable by histopathology and molecular profiling. Expression profiling of patient samples enabled their categorization into molecular subtypes referred to as luminal A, luminal B, Her2 positive, basal-like, and claudin-low (Herschkowitz et al., 2007; Perou et al., 2000). These divisions identify critical differences in cellular composition and molecular pathways, suggesting treatment options and correlating with patient survival (Prat and Perou, 2011). Prognostic expression signatures, refined by related approaches, are being tested or used clinically (Fan et al., 2011; Paik et al., 2006; van 't Veer et al., 2002; van de Vijver et al., 2002). Previously reported prognostic signatures and subtype designations identify a limited set of biologic programs correlating with hormone receptor status (estrogen receptors [ER] and progesterone receptors [PR]) and Her2 expression and proliferation (Desmedt et al., 2008; Fan et al., 2006; Haibe-Kains et al., 2008; Prat and Perou, 2011; Sotiriou and Piccart, 2007). While hormone receptors and Her2 are therapeutic targets, many breast cancers, including most of the basal-like subtypes, lack ER, PR, and Her2 expression and associated targeted treatment options (Pal et al., 2011).

Stem cell biology offers promise for understanding the origins and progression of breast and other cancers and may also reveal the next generation of molecular targets for breast cancers not susceptible to current agents. For example, basal-like breast cancers are poorly differentiated and exhibit gene expression similarities to embryonic and induced pluripotent stem cells (Ben-Porath et al., 2008; Mizuno et al., 2010). Expression profiles derived from adult mammary cells of different differentiation stages have also been used to designate cancers as stem-like or nonstem-like (Lim et al., 2009; Lim et al., 2010; Perou et al., 2010). Breast cancer cells that generate xenografted tumors with high efficiency, regenerate the cellular complexity of the originating tumor, and self-renew (as defined by secondary transplantation) exhibit properties attributed to stem cells and have consequently been called breast cancer stem cells (Al-Hajj et al., 2003). However, defining potential relationships between stem-like cells in breast cancer and normal mammary stem cells (MaSCs) requires MaSC isolation and characterization.

Adult MaSCs (aMaSCs) have been enriched via stem cell isolation methods, and their gene expression signatures have been reported (Lim et al., 2009; Lim et al., 2010; Pece et al., 2010; Raouf et al., 2008; Shackleton et al., 2006; Stingl et al., 2006). However, aMaSC rarity combined with the cellular complexity of the adult gland make purification challenging (Shackleton et al., 2006; Stingl et al., 2006), and copurifying stroma and differentiated mammary cells complicate elucidation of their core self-renewal and differentiation programs.

The developing mammary gland is less complex than the adult gland, suggesting that it may facilitate stem cell identification and purification. Furthermore, while the extensive proliferation, migration, and invasion required for mammogenesis do not occur in the resting adult mammary gland, they do resemble

processes mediating breast cancer progression (Veltmaat et al., 2003). These observations suggest that stem cells present in fetal mammary rudiments (i.e., fetal mammary stem cells [fMaSCs]) might express genes comprising pathways overlooked by analyses focused only on the adult mammary gland and that fMaSCs may reveal new targets to aide detection, prognosis, and treatment of breast cancers. Consistent with this idea, gene expression profiling of bulk epithelium from early mammogenesis revealed significant differences with the adult epithelium (Wansbury et al., 2011). Importantly, this study did not assess whether the profiled cells exhibited stem cell activity, so the relevance of these signatures to fMaSCs remains to be determined.

Mouse mammary gland development begins at approximately embryonic day (E)11.5 with a thickening of the ventral ectoderm to generate five pairs of mammary placodes. The placodes become spherical buds by E12.5, which elongate into ductal sprouts in females by E16 (Veltmaat et al., 2003). Invasion of the extending rudiment into the fat pad precursor begins by E16.5, and by E18.5 the mammary rudiment constitutes a primitive branched network within the mammary fat pad (Veltmaat et al., 2003).

Classic rudiment transplantation studies suggest that mammary stem cells may arise coincident with the morphologic specification of the mammary gland (Sakakura et al., 1979). For example, transplanting multiple intact E13 to E17 epithelial rudiments generated full mammary outgrowths (Sakakura et al., 1979). Heterotypic recombination experiments involving salivary mesenchyme demonstrated that the mammary epithelium is committed to develop into a mammary phenotype by E12.5 (Cunha and Hom, 1996).

Here, we quantify and characterize fMaSC activity during fetal mammogenesis, and analyze the relationships between their gene expression programs and those found in human breast cancer. Our data reveal the unexpected finding that fMaSCs are extremely rare in early embryogenesis but increase rapidly as the mammary rudiment invades into the fat pad precursor. We also show that fMaSCs and their associated stroma exhibit gene expression programs related to those found in specific forms of human breast cancer.

RESULTS

Mammary Stem Cells Are Rare Early but Increase Dramatically during Late Fetal Mammogenesis

We used limiting dilution transplantation analyses (LDTA) to measure mammary repopulating unit (MRU) frequency by using single-hit Poisson statistical analyses (Bonnefoix et al., 1996; Hu and Smyth, 2009; Stingl et al., 2006). Accordingly, fetal mammary repopulating units (fMRU) must contain an fMaSC but may additionally require other cells or components for mammary outgrowth. However, as a single stem cell can generate a mammary gland (Shackleton et al., 2006), we will refer to fMaSC frequency when quantifying fMRUs.

We transplanted limiting dilutions of rudiment-derived cell suspensions obtained at different developmental stages of CD1 embryos into immune compromised CB17-SCID recipients (Figure 1A, Table 1, and Table S1, available online) and in parallel transplanted intact mammary rudiments including surrounding mesenchyme (Figures S1A and S1D). Single intact mammary rudiments from as early as E12.5 transplanted at frequencies >70%. In contrast, measurable fMaSC activity was not evident in dissociated bulk mammary cell populations prior to E15.5 (Figure 1A, Table S1D, Table 1, column 2, Table S1, column 3, and Table S2). This was surprising as we transplanted 10,000 viable cells (epithelial and mesenchymal) per fat pad, which is more than we estimate to be present in a single rudiment (Figure 1A, Table 1, and Table S1, column 3). While rudiment dissociation could have reduced repopulation efficiency, especially if contextual cues analogous to niche interactions (Spradling et al., 2001) are required for stem cell function, identically dispersed E18.5 rudiment cells routinely generated mammary outgrowths from 100 cells (Table S1, column 3). Thus, fMaSC concentration increases dramatically during fetal development (Figure 1A; Table 1, column 2, and Table S1, column 3).

The importance of extracellular cues in stem cell function (Spradling et al., 2001) prompted us to determine whether Matrigel would increase fMaSC transplantation efficiency as it does aMaSCs (Lim et al., 2009). While Matrigel significantly increased the sensitivity of fMaSC detection, it still equated to one or fewer stem cells per E13.5 rudiment (1/12,000 cells; Figure 1A, Table 1, column 3, and Table S1, column 4). fMaSC activity peaked at E18.5, increasing to 1 in 60 cells with Matrigel, a 14-fold increase compared to transplantation in its absence (Figure 1A, Table 1, and Table S1). Thus, fMaSC concentration increases at least 200-fold between E13.5 to E18.5 when measured in the presence of Matrigel (Figure 1A and Table 1, column 3). This reflects a striking 9-fold increase in fMaSC abundance during the narrow developmental window between E15.5–E16.5 (1 in 1,800 to 1 in 200, $p < 0.001$) (Figure 1A, Table 1, and Table S1).

These quantitative measurements of stem cell frequency during embryogenesis reveal for the first time the surprising finding that transplantable fMaSCs are rare early in mammogenesis but are abundant late. Furthermore, the fMaSC frequency in unfractionated E18.5 embryonic mammary rudiments is ~5-fold higher than that obtained with bulk adult mammary cell populations measured under identical conditions (1 in 60 versus 1 in 300, $p < 0.001$) (Table 1 and Table S1). These differences may, in part, reflect different contaminating epithelial and stromal components within the cell populations obtained at different stages. Nevertheless, the data indicate that mammary stem cell frequency is higher in the E18.5 mammary rudiment than in the adult gland. This facilitates their purification for subsequent molecular analyses.

Stem Activity Is Restricted to a Unique Fetal Population Expressing High Levels of CD24 and CD49f

aMaSCs can be enriched with fluorescence activated cell sorting for surface markers such as CD24 (heat stable antigen [HSA]) and CD49f (α6 integrin) (Stingl et al., 2006). Both proteins were expressed in the stromal and epithelial compartments of E13.5 and E15.5 mammary rudiments (Figure 1B). In contrast, high CD24 and CD49f expression at E18.5 identifies a basal-epithelial compartment with negligible staining in the fat pad and surrounding mesenchyme, suggesting the utility of these markers for fMaSC enrichment (Figure 1B). Consistent with

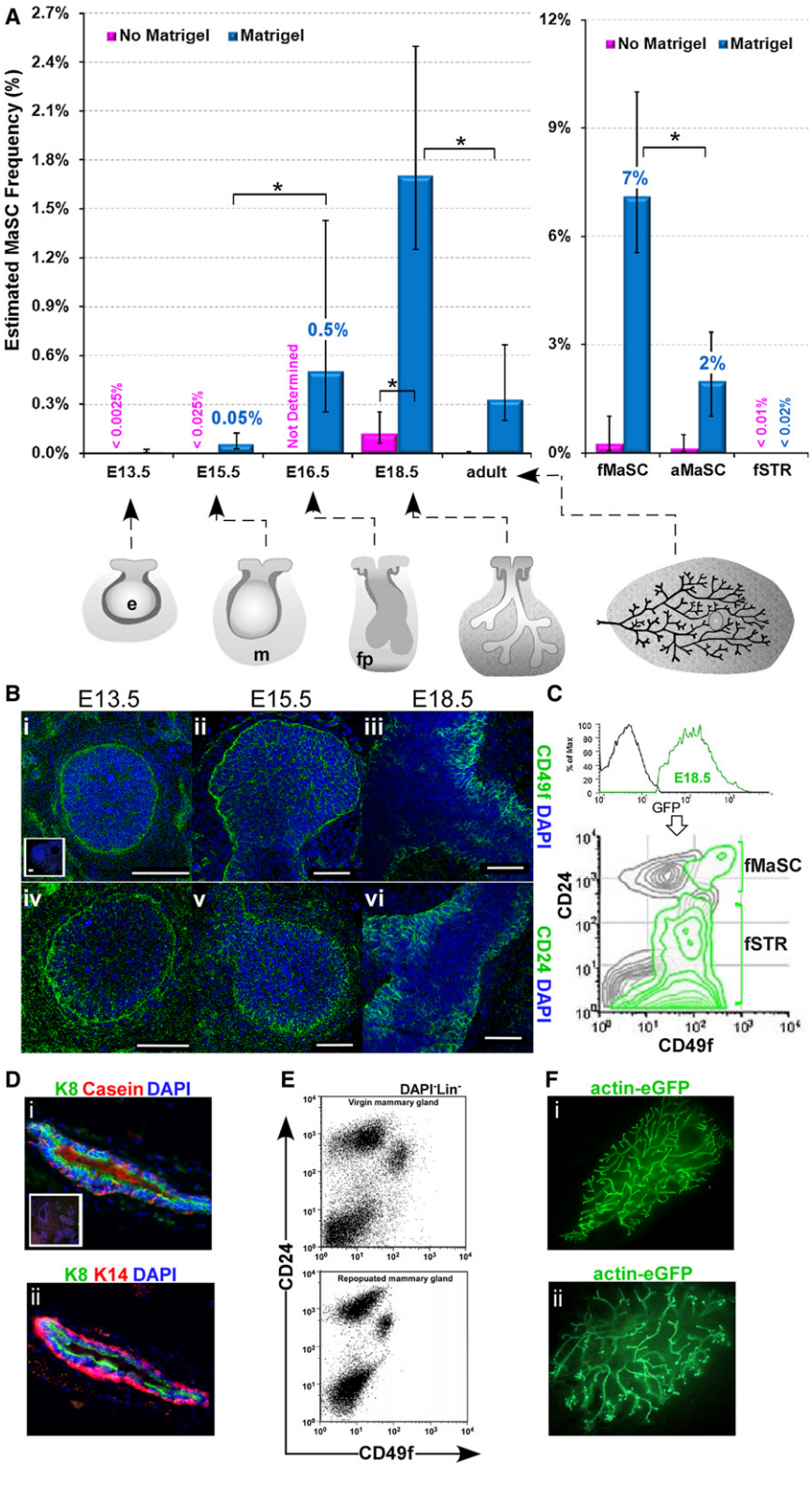

Figure 1. fMaSCs Identified in Late Embryogenesis Express High Levels of CD24 and CD49f

(A) Mammary stem cell frequency estimates at various stages of fetal development and in the adult in the presence or absence of Matrigel. Gross morphological appearance of the gland at various stages is illustrated. The following abbreviations are used: e = epithelium, m = mesenchyme, and fp = fat pad. *p < 0.001, pairwise group difference. The error bars indicate 95% confidence intervals (CI).

(B) Confocal images showing CD49f (i–iii) and CD24 (iv–vi) expression in whole mounts at E13.5, E15.5, and E18.5.

(C) Histogram and FACS contour plot showing the distribution of cells expressing CD24 and CD49f in the LIN$^-$ population (DAPI$^-$CD31$^-$CD45$^-$TER119$^-$) in mammary glands from a nulliparous adult mouse (black) and actin-eGFP E18.5 female embryos (green). Adult eGFP$^-$ mammary and eGFP$^+$ E18.5 fetal mammary cell suspensions were mixed, costained, and analyzed together.

(D) Immunofluorescence analysis of paraffin sections of a regenerated mammary gland from a parous recipient showing casein/K8 (i) and K14/K8 (ii). The inset shows a secondary antibody control.

(E) Representative FACS dot plots showing very similar patterns of expression of CD24 and CD49f in viable lineage-depleted mammary cells from a nulliparous adult mouse (top) and from a mammary gland regenerated by the fMaSCs (bottom).

(F) Representative whole mount of actin-eGFP mammary outgrowth arising from transplantation of the fMaSC population (Lin$^-$CD24^{high}CD49f^{high}) isolated from E18.5 embryos. The mammary glands were harvested from primary (i) and secondary (ii) recipients 12 weeks after transplantation. See also Table 1, Table S1, and Figure S1.

this, flow cytometry demonstrated that most E13.5 and E15.5 rudiment cells expressed CD24 and CD49f (Figure S1B). At E18.5, however, these markers delineate a distinct subpopulation comprising approximately 5% of the cells following the exclusion of endothelial and hematopoietic lineages (Figure 1C and Figure S1B). We then compared the CD24 and CD49f staining profiles of admixed and coprocessed eGFP$^-$ adult and eGFP$^+$ E18.5 fetal mammary cells (Figure 1C). Cells derived from E18.5 rudiments express higher levels of CD24 than the previously reported CD24^{med}CD49f^{high} aMaSC-enriched population and higher levels of CD49f than the CD24^{high}CD49f^{low} adult luminal CFC population (colony-forming cells) (Figure 1C) (Stingl et al., 2006). This direct comparison with adult mammary cells shows that the fetal population is CD24^{high}CD49f^{high}.

The CD24^{high}CD49f^{high} subpopulation contained all fMaSC activity by transplantation analyses (Figure 1A and Table 1).

Table 1. Fetal Mammary Rudiments in Late Embryogenesis Are Found to Be Highly Enriched with Mammary Stem Cells

	MaSC Frequency (95% CI)	
Bulk Mammary Cells	No Matrigel	Coinjected with Matrigel
E13.5[a]	**<1/40,000**	**1/12,000** (1/5000 to 1/30,000), p = 0.2
E15.5[a]	**<1/4,000**	**1/1,800** (1/800 to 1/4,000), p = 0.9
E16.5[a]	ND	**1/200** (1/70 to 1/400), p = 0.68
E18.5[a,b]	**1/830**[c] (1/400 to 1/1,600), p = 0.8	**1/60**[c] (1/40 to 1/80), p = 0.7
Adult[b]	**1/30,000**[d] (1/11,000 to 1/80,000), p = 0.2	**1/300** (1/150 to 1/500), p = 0.2
Fetal MaSC population ($CD24^{high}CD49f^{high}$)	**1/400**[d] **(1/100 to 1/1,700),** p = 0.2	**1/14**[c] (1/10 to 1/18), p = 0.7
Fetal fSTR population ($CD24^{med/low/neg}$)	**<1/9,000**	**<1/5,000**[e]
Adult MaSC population ($CD24^{med}CD49f^{high}$)	**1/800**[d] **(1/200 to 1/2,700),** p = 0.4	**1/50** (1/30 to 1/100), p = 0.98[e]

p > 0.05 for frequency estimates indicates the data are consistent with a single-hit Poisson model. ND is an abbreviation for not determined.
[a] p < 0.001, pairwise group difference.
[b] p < 0.001, pairwise group difference.
[c] p < 0.001, pairwise group difference.
[d] These values represent rough MaSC frequency estimate (see Statistical Analyses for detail).
[e] p < 0.001, pairwise group difference.

The remaining fetal population exhibits lower CD24 levels, is devoid of fMaSC activity, and is enriched in stromal cells as defined by cellular morphology and protein and gene expression analyses (see below). Therefore, we call this population the fetal stroma-enriched population (fSTR). As few as five to ten fMaSCs reproducibly enabled robust mammary gland repopulation, while up to 3,000 cells from the fSTR consistently failed to generate outgrowths, even with Matrigel addition (Figure 1A, Table 1, and Table S1). We estimate the stem cell frequency in the fMaSC-enriched population to be 1 in 14 with Matrigel (Table 1, Table S1, and Figure 1A), which is an ~4-fold enrichment over the aMaSC frequency when immune-compromised hosts were used in the presence of Matrigel (1/50 [aMaSC] versus 1/14 [fMaSC], p < 0.001; Table 1 and Table S1). Importantly, the aMaSC frequency in Matrigel when allotransplantation into immune-compromised hosts was used was similar to that obtained with an immune competent, syngeneic model (C57BL6) in the absence of Matrigel (Tables S1 and S3), and host immune competence did not significantly affect fMaSC frequency in the presence of Matrigel (Table S3).

fMaSCs generated morphologically normal, fully arborized ductal structures that produced casein-positive alveolar structures upon induction of pregnancy (Figure 1D). Mammary outgrowths exhibited the expected localized expression of luminal and myoepithelial keratins (K8 and K14, respectively) (Figure 1D), the phenotypic cellular heterogeneity of wild-type adult mammary glands (Figure 1E), and contained cells able to self-renew based on serial transplantation analyses (Figure 1F). Thus, the fMaSC-enriched population exhibits the multi-lineage cell differentiation and self-renewal characteristics expected of mammary stem cells, but at considerably higher concentration than found in the adult (Shackleton et al., 2006; Stingl et al., 2006).

fMaSCs Are Multipotent and Coexpress Markers of Multiple Mammary Lineages

We evaluated the ability of individual fMaSCs to generate multiple lineages in vitro (Dontu et al., 2003). While fMaSCs had negligible sphere-forming efficiency (SFE) with a conventional nonadherent sphere-forming protocol at low seeding density (1,000 cells per cm^2) (SFE ~0.1%; Figures 2A and 2B), fSTR formed numerous spherical clusters under identical conditions (SFE = 1.4%) (Figures 2A and 2B). However, just as Matrigel profoundly increased transplantation efficiency, even low percentages of Matrigel (2%) enabled the fMaSC population to generate spheres with an SFE of 9.4% when plated at low density (Figures 2A and 2B). The primary fMaSC-derived spheres were morphologically similar to the colonies previously reported for the aMaSC population (Figure 2A) (Stingl et al., 2006). In addition, fMaSC-derived primary spheres expressed markers associated with both myoepithelial (e.g., cytokeratin 14 [K14]) and luminal (cytokeratin 8 [K8]) epithelial lineages of the mammary gland (Figure 2C).

We used two independent strategies to determine whether primary spheres arise from clonal expansion from a single cell or from cell aggregation. First, we seeded single cells from the fMaSC population into individual wells. Primary spheres formed (SFE = 10.7%) in 2% Matrigel, similar to the 9.4% SFE observed when the cells were plated at low density (Figure 2B and Figure S2A). Secondary and tertiary spheres were also formed with similar SFEs (~10%; Figure 2B). The fSTR did not generate spheres in the presence of Matrigel and instead produced cultures of dispersed cells resembling fibroblasts and neurons (Figures 2Aii and 2B). Second, we mixed single-cell suspensions of $eGFP^+$ and $eGFP^-$ cells from the fMaSC population and then grew them at low density (Figure 2B and Figure S2B). As 199 out of 200 spheres were a single color, the vast majority must derive from single cells (Figure S2C). Approximately 60% of fSTR-derived clusters were overtly polyclonal when cultured in nonadherent conditions without Matrigel (Figure 2Aiii), indicating they arise by aggregation. Taken together, these data show that ~10% of the fMaSC population exhibits the stem cell properties of multipotent differentiation and self-renewal in vitro (Figures 2B and 2C).

Coexpression of proteins associated with multiple lineages has been proposed to indicate plasticity in the normal mammary gland and in breast cancers (Creighton et al., 2009; Livasy et al., 2006; Petersen and Polyak, 2010; Sun et al., 2010; Thomas et al., 1999). We detected cells that coexpress K14 and K8 from

as early as E13.5 in the developing mammary gland (Figure S2D and S2E). Approximately 30% of the cells within the fMaSC population were $K14^+K8^+$, and we frequently detected such double-positive cells in fMaSC-derived spheres (Figures 2C and 2D). We also analyzed vimentin expression as it has been associated with the myoepithelial and mesenchymal lineages of the normal mammary gland and with aggressive disease when coexpressed with luminal epithelial markers in breast cancer patients (Creighton et al., 2009; Thomas et al., 1999). Approximately 70% of cells within the $K14^+K8^+$ fMaSC population also expressed vimentin (Figure 2D).

Derivation of fMaSC- and fSTR-Specific Gene Expression Signatures

We performed microarray expression analyses on the fMaSC, fSTR, and aMaSC populations to ascertain molecular pathways with potential relevance to fetal mammary development, fMaSC biology, and breast cancer. We obtained reproducible expression profiles from independent biological pools representing each population and identified differentially expressed genes comprising fMaSC, fSTR, and aMaSC signatures (Figure 3A and Table S4; significance analysis of microarrays; false discovery rate (FDR) < 10%; [Tusher et al., 2001]). We identified 869 unique genes more highly expressed in the fMaSC population (the fMaSC signature) than in the fSTR and 812 unique genes more highly expressed in the fSTR population (the fSTR signature) than in the fMaSC. Among the fMaSC signature genes, ~34% were common to both the fMaSC and aMaSC populations when compared to fSTR, but ~40% were significantly overexpressed in the fMaSC relative to the aMaSC (Figure 3A).

We confirmed the differential gene expression patterns between the fMaSC and fSTR populations on a panel of genes selected from putative stem cell, developmental, and cancer relevant pathways (Figures 3B and 3C). Furthermore, high-throughput single-cell qRT-PCR analyses confirmed expression of a partially overlapping selection of 46 genes in individual cells of the fMaSC population (Figure 3D). This approach also verified that individual fetal cells coexpress luminal keratins, myoepithelial keratins, and vimentin (Figure 3D).

Unique Expression Features of fMaSCs and fSTR

Many well-studied genes were found to be expressed in a manner consistent with the cell types analyzed, indicating the validity of the microarray data (Table S4). However, the fMaSC and fSTR signatures revealed unique gene expression patterns when compared to adult mammary populations or to those isolated earlier in development that we showed to be lower in stem cell content than the fMaSC population (Figures 1 and 4, Table 1, and Tables S4 and S5). For example, qRT-PCR analysis showed significant differences in expression of specific stem cell- and development-related genes between the fMaSC and the E15.5 rudiment (Figure 4A). The gene content in the E18.5 fMaSC and fSTR signatures were also significantly different from those reported for either mouse or human adult mammary populations, or from E12.5 mouse mammary epithelia (ME) and mammary mesenchyme (MM) (Figures 4B–4D and Tables S4 and S5) (Kendrick et al., 2008; Lim et al., 2009; Lim et al., 2010; Pece et al., 2010; Stingl et al., 2006; Wansbury et al., 2011). Although the similarities between the fMaSC and previously reported primary mammary epithelial signatures are statistically significant, the majority of genes in the fMaSC signature are not represented in aMaSC signatures (Figure 4B). Surprisingly, the fSTR signature is similar to the adult mammary stromal signature and to published aMaSC signatures (Figure 4B).

We delineated genes specific to the fMaSC and fSTR populations by comparing their signatures to composite human/mouse adult MaSC or stromal gene lists and to E12.5 ME and MM signatures (Figure 4C). The sets of genes specific to the fMaSC and fSTR signatures are rich in biological content as indicated by their significant correlation with numerous gene ontology (GO) categories (Figure 4D, Figure S4, and Tables S4 and S6). Among these, cell signaling and genes associated with the plasma membrane figure prominently (Figure 4D). A selection of the most highly enriched clusters are detailed in Figure 4D, including several genes previously implicated in mammary stem cell function and breast cancer, such as *ErbB2* and *ErbB4* (Korkaya and Wicha, 2009). Several genes reciprocally expressed in the fSTR and fMaSC populations are suggestive of paracrine signaling and may contribute to stem cell behavior in normal or neoplastic growth. For instance, the fSTR specific signature includes *Nodal* and *Wnt5a*. Nodal is a TGF-β family morphogen that can promote oncogenic phenotypes in mammary cells and has been implicated in breast and other cancers (Strizzi et al., 2009). The Wnt5a protein is a noncanonical Wnt implicated in polarity, migration and stem cell maintenance (Kikuchi et al., 2012). Additional processes found in both the fMaSC and fSTR populations are likely to contribute to the unique properties of mammary cells at this stage. For example, changes in chromatin regulation, augmented synthetic metabolism and cell cycle, and the production of distinctive extracellular matrices may contribute to the robust fMaSC function we observe (Figure S4 and Table S4).

Cellular Interaction Is a Predicted Hallmark of fMaSC Function

GO enrichment analysis of fetal signatures suggested a prominent role for cell-cell and cell-niche interactions, including cell surface receptor signaling in the fMaSC population (Figure 4 and Table S4). We used curated interaction networks in the GeneGo pathway analysis platform to organize the genes comprising the fMaSC and fSTR signatures into potential receptor-ligand interactions. This enabled construction of a hypothetical interaction map based on reported receptor-ligand interactions (Figure 5A).

We determined whether predicted pathways are relevant for fMaSC function in vitro (Figures 5B–5D and Figure S5). We analyzed ErbB and FGF receptors and their ligands given their cancer relevance and that growth of adult mammary epithelial cells in vitro requires either EGF or FGF (Dontu et al., 2003). qRT-PCR validated the differential expression of all four ErbB family members, and the hormone receptors ER and PR (Figure S5A, and data not shown). *ErbB4* was expressed at a low level but exclusively in the fMaSC population (data not shown). *ErbB2* and *ErbB3* were expressed more highly in the fMaSC population than either the fSTR or aMaSC populations (Figure S5A), and ErbB2 protein was detected in situ in CD24+ cells in E18.5 mammary rudiments (Figure S5B).

We examined the requirement for ErbB and FGF signaling by growing fMaSC-derived spheres in 2% Matrigel culture

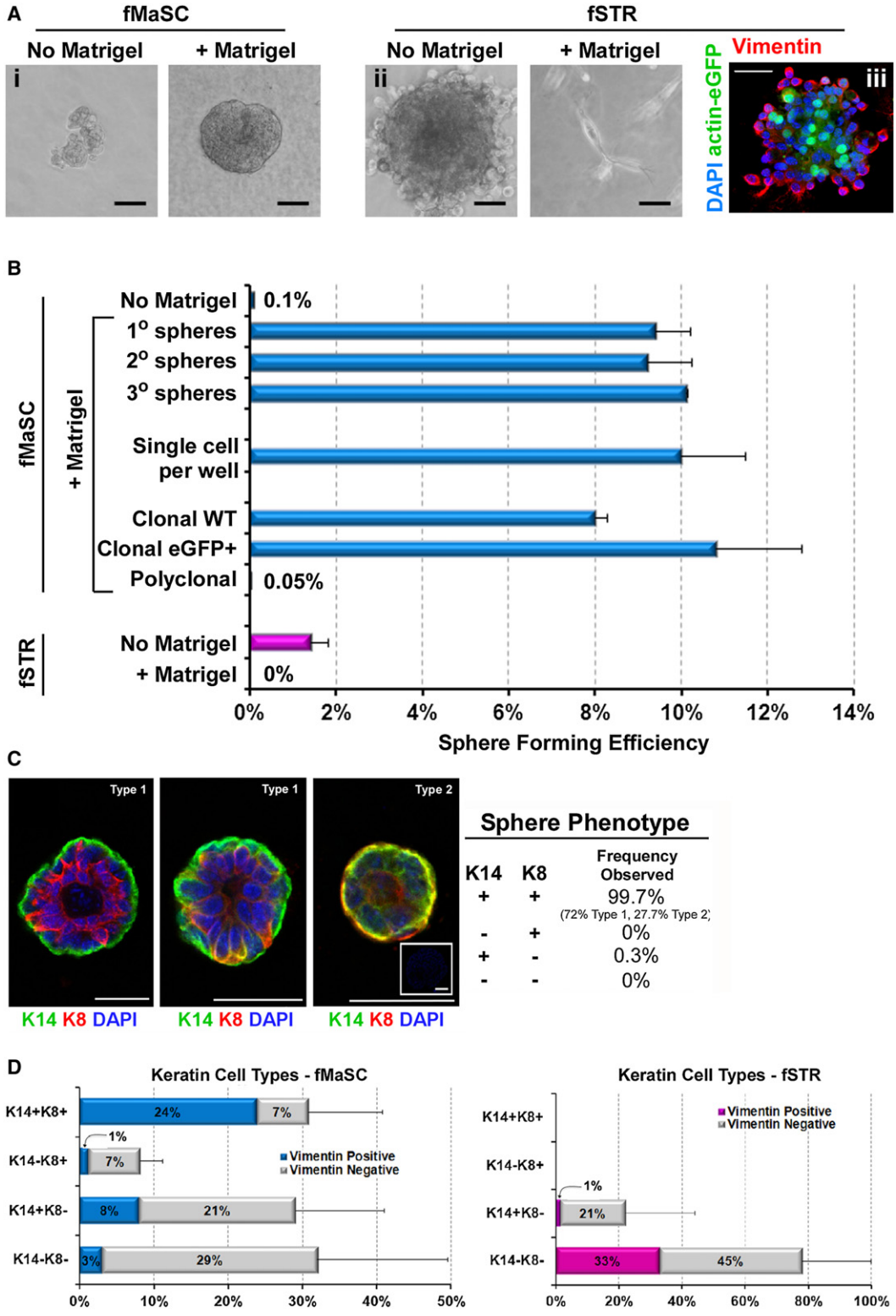

Figure 2. Individual Cells from the fMaSC Population Generate Clonal, Multilineage Spheres that Can Be Serially Propagated and Coexpress Markers of Multiple Lineages

(A) Morphology of structures generated from fMaSC (i) and fSTR (ii) populations grown under nonadherent conditions in vitro in the presence and absence of Matrigel. (iii) Confocal image of an fSTR polyclonal sphere derived by mixing fSTR cells from WT and actin-eGFP transgenic embryos showing vimentin immunofluorescence (red), nuclear counterstain DAPI (blue), and actin-eGFP (green). The scale bar represents 50 μm.

containing or lacking specific ErbB ligands and FGF. Cultures lacking both EGF and FGF produce no spheres, while either EGF or FGF stimulated fMaSC-derived sphere formation (Figure 5B). Heregulin 1 (Hrg1, neuregulin, Neu differentiation factor), an ErbB ligand with a preference for ErbB3 or ErbB4, stimulated sphere growth in the absence of EGF and FGF (Figure 5B) (Britsch, 2007). The effects of these ligands were additive (SFE ~10% for EGF/FGF/HRG), and Hrg1 showed the most dramatic effect on large sphere production (Figure 5B). By contrast, GDNF, which is not represented in the hypothesized interaction network, did not stimulate sphere formation (Figure 5B).

Consistent with the above results, ErbB and FGFR kinase antagonists inhibited fMaSC-derived sphere growth (Figures 5C and 5D and Figure S5). Lapatinib is a reversible and highly specific ErbB1/2 dual tyrosine kinase inhibitor (Rusnak et al., 2001), while neratinib is an irreversible pan-ErbB kinase inhibitor (Rabindran et al., 2004). Lapatinib and neratinib inhibited sphere growth with a similar dose-dependence as observed for Her2 overexpressing human mammary cells with documented sensitivity to these agents (Figures 5C and 5D) (Wang et al., 2006). As these drugs have nonoverlapping potential off-target effects (Karaman et al., 2008; Rabindran et al., 2004; Rusnak et al., 2001), it is most likely that their effects on sphere growth derive from ErbB pathway antagonism. However, it remains to be determined whether inhibition of one specific ErbB receptor accounts for the observed effects on sphere growth or whether redundancy in this family necessitates inhibition of multiple receptors for effective fMaSC growth antagonism in vitro. Altogether, these findings substantiate the importance of ErbB and FGF signaling in fMaSC-derived sphere growth in vitro, and they indicate the presence of functionally relevant gene content in the microarray-derived fetal mammary signatures.

Molecular Links between Fetal Mammogenesis and Breast Cancer

Cancer-associated genes (*ErbB2*, *Met*, *CXCR4*, etc.) were prominent among the fetal signatures and pathway analyses and in unsupervised gene set enrichment analyses (Figures 4 and 5, Figure S5, and Table S4). Therefore, we determined whether fetal gene expression signatures were enriched in particular human breast cancer intrinsic subtypes by using archival tumor microarray data from two independent compendia and human orthologs of the fMaSC and fSTR signature genes (Figure 6, Figure S6, and Table S6) (Ben-Porath et al., 2008; Prat et al., 2010). Enrichment for the fMaSC signature was concentrated among tumors designated as basal-like, which tend to be poorly differentiated and stem-like (Ben-Porath et al., 2008; Mizuno et al., 2010). In addition, many Her2$^+$ tumors showed significant enrichment for the fMaSC signature (Figure 6A and Figure S6A). Enrichment for the fSTR signature often correlated with tumor subtypes characterized by low proliferation and favorable prognoses (Figure 6A and Figure S6A) (Sørlie et al., 2001). However, claudin-low and metaplastic-like tumors, which have also been suggested to be stem-like (Hennessy et al., 2009; Perou et al., 2010; Prat et al., 2010) were generally enriched for the fSTR signature and depleted for the fMaSC signature (Figure 6A and Figure S6A). Breast cancers showing enrichment for fSTR signatures showed nearly identical enrichment patterns for aMaSC signatures (Figure S6B), consistent with the significant gene overlap of aMaSC and fSTR signatures noted above (Figure 4B).

Previous studies have used signatures derived either directly from breast cancer array data or from specific biological contexts, such as serum stimulation of fibroblasts (simulating wound healing), to classify breast cancers into different tumor types with distinct clinical features (Fan et al., 2006). The fMaSC signature exhibits relatively little overlap with these signatures (6.5% of fMaSC genes shared, Figure 6B and Table S7). While, the signatures compared in Figure 6B have significant representation of ER- and/or proliferation-associated genes (Fan et al., 2006; Wirapati et al., 2008), the fMaSC and fSTR signatures have little representation of proliferation genes (Figure 6B) because this is a characteristic they share, leading to exclusion from their comparative profiles. Furthermore, removal of the few residual proliferation-related genes from the fMaSC and fSTR signatures did not markedly alter the observed tumor enrichments (Figure 6A and Figure S6A). We cannot rule out the possibility that fetal-like molecular programs are also invoked by other proliferative states in the mammary gland, for instance at puberty or pregnancy or during outgrowth of transplanted material. Regardless, the fMaSC and fSTR signatures clearly identify a distinct group of genes associating fetal mammary gland biology and fMaSCs with specific molecularly defined breast cancer subtypes (Figure 6B).

Fetal Gene Subsets Identify Patients with Diverse Prognoses in Archival Tumor Samples

The fMaSC and fSTR signatures can be subdivided into gene expression modules showing coordinated expression across multiple tumors with hierarchical clustering analysis (Figures S6C and S6D). We then correlated these subsignatures with breast cancer grade, progression, subtype, or prognosis (Figure 6C and Figures S6 and S7). We subdivided the fMaSC and fSTR signatures into five and four subsignatures, respectively, by using the 96 genes with the greatest variance in the compendium. The genes comprising these enriched subsets represent diverse biological processes previously implicated in cancer, including immune response (fMaSC-iii, fSTR-ii), cell survival (fMaSC-v), and wounding (fSTR-ii, fSTR-iv) (Figures 6C and 6E and Table S7) (Chang et al., 2004; Perou et al., 2000; Rody

(B) Quantification of clonal, primary fMaSC-derived sphere growth, secondary and tertiary sphere growth, and fSTR-derived sphere growth. The error bars indicate standard deviation (SD).
(C) Confocal immunofluorescence analysis of spheres derived from the fMaSC population showing the expression of K8 (red), K14 (green), or both (yellow) with nuclear counterstain DAPI (blue) and tabular summary of sphere types observed. Type 1 spheres consist of cells expressing either K14 (i.e., sphere periphery) or K8 (i.e., middle of the sphere), while type 2 spheres consist mainly of cells coexpressing K8 and K14 (yellow cells). Inset, secondary antibody control. The scale bars represent 25 μm. The inset shows secondary antibody control (the scale bars represent 50 μm).
(D) Summary of the percentage of cells in the fMaSC and fSTR populations expressing K8, K14, and/or vimentin. The error bars indicate standard deviation. See also Figure S2.

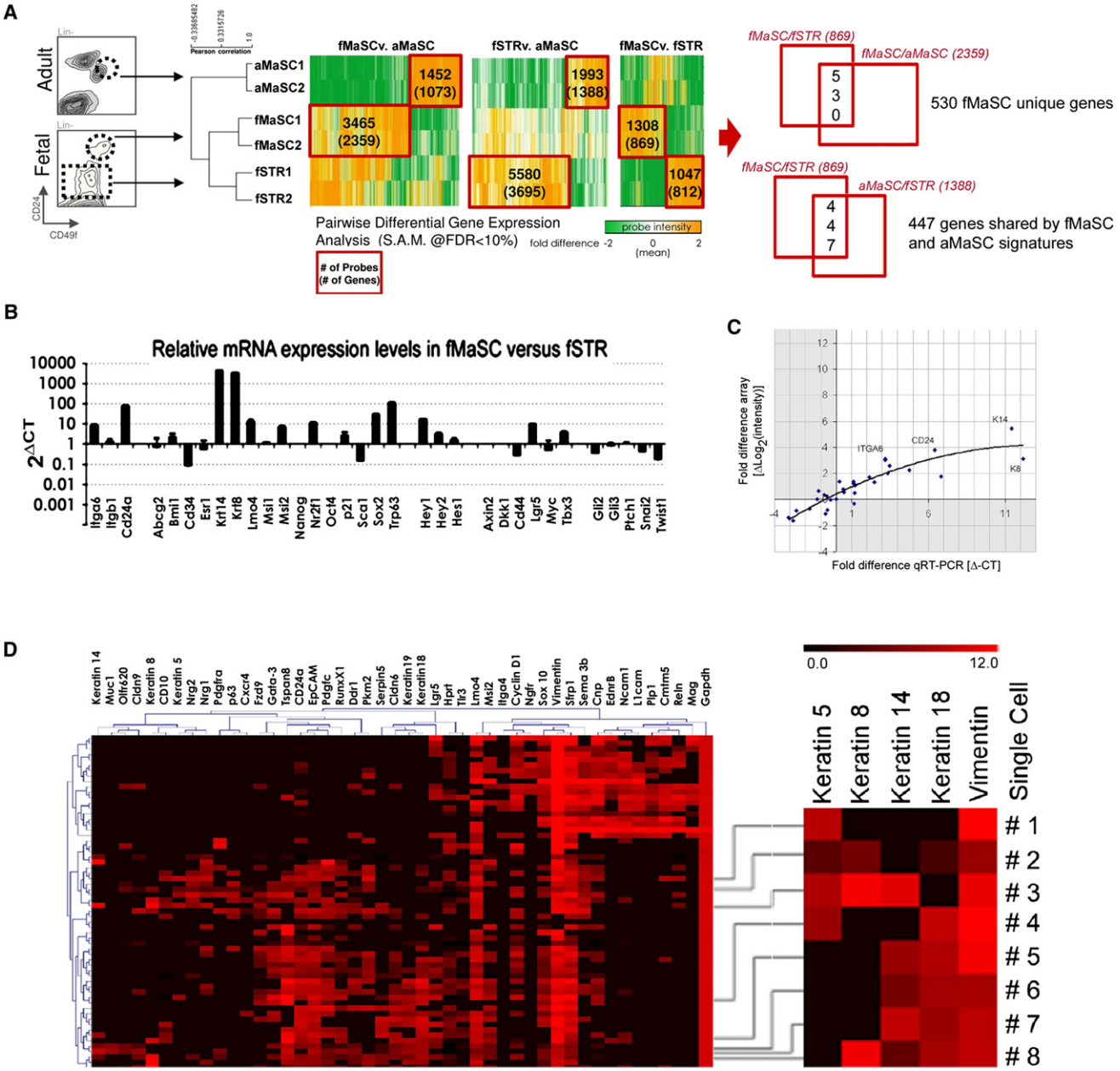

Figure 3. Differential Gene Expression Profiling of fMaSC, fSTR, and aMaSC Populations

(A) Illustration of sorted populations, Pearson correlation among biological replicates for each cell type, and heat maps illustrating the identification of differentially expressed genes (SAM; FDR < 10%).

(B) qRT-PCR analysis of select stem cell and developmental genes in the fMaSC population relative to fSTR. Error bars indicate standard deviation.

(C) Expression levels of a representative selection of genes determined by microarray and by qRT-PCR. The expression level in the fMaSC relative to the fSTR is plotted as the fold difference in expression. Fold differences in gene expression were calculated for RT-PCR assuming ideal amplification (fold change = $2^{\Delta Ct}$) and for Nimblegen array data with the normalized probe intensities (fold change = ΔLog_2(intensity)). Data were normalized to hypoxanthine-guanine phosphoribosyltransferase. Despite differences in the dynamic range of the two techniques, the pattern of differential expression between the fMaSC and fSTR determined by array was consistent with the pattern determined by qRT-PCR.

(D) Microfluidics-based, single-cell, qRT-PCR analyses of cells from the fMaSC population. Right: examples of single cells coexpressing various keratins and the mesenchymal marker, vimentin. See also Table S4.

et al., 2011). Other process such as embryonic morphogenesis (fMaSC-ii, fMaSC-v, and fSTR-iii) and adhesion (fMaSC-iv and fSTR-iii), which have been less extensively investigated in cancer, were also represented (Figure 6E and Table S7).

These fetal subsignatures exhibit prognostic relevance in archival breast cancer array data (Figures 6C and 6D and Figure S7). For instance, enrichment for signature fMaSC-ii or repression of signature fSTR-iv correlated with Her2^{+} and

basal-like tumors, high grade, and reduced probability of patient survival (Figure 6C and Figure S7). This observation is consistent with the predicted outcome of these intrinsic subtypes (Sørlie et al., 2001). In addition, multivariate survival analyses based on enrichment for the fetal subsignatures showed prognostic value beyond commonly used clinical metrics such as ER status, tumor size, grade, and lymph node status (Figure 6D). The biological and prognostic relevance of the signatures described here is a function of their biological origin, as randomized signatures are not enriched in a sufficient number of tumors to enable tumor classification and subsequent survival analysis (Figure 6A and Figure S7). However, it may be possible to derive alternative fetal gene subsignature groupings exhibiting enhanced prognostic value, predictive value, or additional functional biological insight through the use of alternative statistical approaches. As approximately 60% of the genes comprising these fetal subsignatures are specifically upregulated relative to the aMaSC population (Tables S4, S5, and S7), these signatures provide new candidates for therapeutic and prognostic strategies that would probably be missed by deriving signatures from the resting adult gland.

DISCUSSION

The existence of fMaSCs has been inferred from studies demonstrating that intact mammary epithelium obtained from as early as E13.5 can fully reconstitute the mammary gland (Sakakura et al., 1979). However, these studies did not quantify or purify mammary stem cells. This left a substantial gap in our understanding of mammary biology and precluded elucidation of the long predicted molecular and genetic links between fetal mammary development, stem cells, and breast cancer (Howard and Ashworth, 2006). Here, we provide the first quantitative assessment of mammary stem cell activity during fetal mammogenesis, obtain fetal mammary gene expression profiles and evaluate their relationship to breast cancer.

Our studies reveal the surprising finding that mammary rudiments from E15.5 and earlier contain few if any functional fMaSCs. We observed a 200-fold increase in fMaSC activity during the course of fetal mammogenesis that parallels the change in cellular context as the proliferating mammary epithelium begins to invade through the adjacent mesenchyme and interacts with the fat pad microenvironment (Veltmaat et al., 2003). While proliferation during mammogenesis probably contributes to fMaSC abundance, the 9-fold increase in fMaSC frequency between E15.5 and E16.5 is difficult to explain solely by cell division. Instead, we propose that stromal interactions during this interval generate signals that act on precursor cells to engender the stem cell competence we assay by transplantation. It is noteworthy that a recent in vivo lineage tracing study also demonstrated the existence of bipotent mammary stem cells in late embryogenesis and suggested a restriction to unipotent stem/progenitor activity occurring shortly after birth (Van Keymeulen et al., 2011).

The hypothesis that context and extrinsic cues underlie fMaSC functional identity is consistent with studies showing the importance of cell-cell and cell-matrix interactions and locally produced soluble factors for stem cell function (Jones and Wagers, 2008; Spradling et al., 2001). Direct niche interactions also maintain the stem cell state within various tissues and organisms, such as *Drosophila* testes and mammalian hair follicles, bone marrow, testes, and intestines (Spradling et al., 2001). Stem cell niches also produce soluble factors, including Wnt, FGF, TGFβ, and EGF ligands, which promote or maintain the stem cell state (Spradling et al., 2001; Zeng and Nusse, 2010). Importantly, the involvement of multiple ErbB receptors and their ligands in mammary morphogenesis (Jackson-Fisher et al., 2008; Jackson-Fisher et al., 2004; Tidcombe et al., 2003; Wansbury et al., 2011) is consistent with our observations implicating this family in fMaSC function in vitro. The ErbB kinase inhibitor studies reported here and gene knockout studies showing that mammary gland development is impaired to differing degrees in various ErbB knockout mouse strains (Jackson-Fisher et al., 2008; Jackson-Fisher et al., 2004; Tidcombe et al., 2003) suggest that interactions with relevant stromal components and growth factor gradients may be important for inducing stem cell activity during development.

The fMaSC population includes cells that coexpress luminal and myoepithelial markers with vimentin. The expression of vimentin within epithelial cells of the human adult mammary gland is normally restricted to the myoepithelial lineage and has not been reported to occur in concert with luminal keratin expression (Anbazhagan et al., 1998; Mørk et al., 1990). Interestingly, forced coexpression of luminal keratins 8 and 18 with vimentin in human breast cancer cells in vitro increases motility, invasiveness, and proliferation (Hendrix et al., 1997). Similarly, basal-like breast cancers frequently exhibit an undifferentiated phenotype and coexpress myoepithelial and luminal epithelial keratins and vimentin (Livasy et al., 2006). Our data suggest that the coexpression of myoepithelial and luminal keratins and vimentin may typify an uncommitted, embryonic, fMaSC-like state. We suggest that the partial epithelial to mesenchymal transition (EMT) commonly observed during aggressive tumorigenesis may represent a reversion to an embryonic-like state resembling the fMaSC and/or fSTR compartments (Hanahan and Weinberg, 2011). EMT has long been recognized as an essential embryonic process required for development beyond the blastula stage (Hay and Zuk, 1995) and may also promote a stem cell-like state in breast cells (Mani et al., 2008; Thiery and Sleeman, 2006).

fMaSC signatures are derived from cells with a defined biological role and have not been analyzed previously for their relationship to cancer. Other signatures representing biological processes, such as wound healing and immune response, have proven useful for gauging the risk of recurrence in some breast cancer subtypes (Chang et al., 2004; Rody et al., 2011). Thus, we anticipated that our analyses would uncover new genes and pathways related not only to fetal mammary development and fMaSC function but also to breast cancer. Our results suggest that this resource contains new gene sets with prognostic value that may also be useful for predicting which patients will respond to certain treatment strategies. For example, patients receiving ErbB (Her)-targeted therapies, such as herceptin (Trastuzumab) and lapatinib, are selected based on *ErbB2* gene amplification and high-level ErbB2 expression within their tumors (Jacobs et al., 1999). However, in the NSABP-31 clinical trial, some patients confirmed by clinical standards to be ErbB2 negative responded to the ErbB targeted treatment

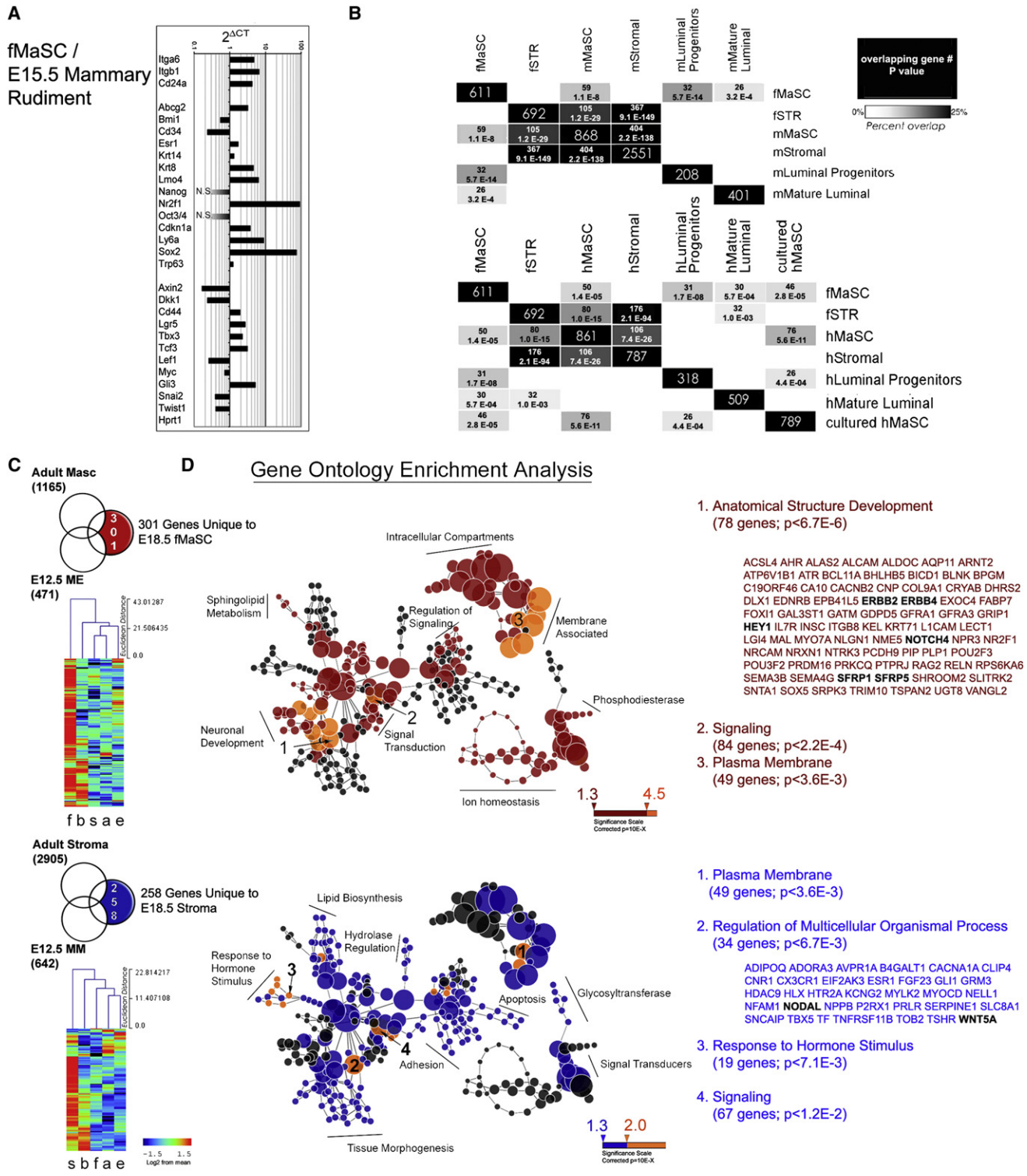

Figure 4. Unique Gene Content in the E18.5 Fetal Mammary

(A) qRT-PCR analysis of select stem cell and developmental genes in fMaSC relative to the E15.5 mammary rudiment. N.S is an abbreviation for no signal.

(B) Overlap of fMaSC signature genes and their orthologs with previously reported normal adult mammary signatures. Upper: mouse signatures (Lim et al., 2009; Pece et al., 2010). Lower: shows hMaSC and hStromal signatures (Lim et al., 2010) and a signature from cultured hMaSCs (Lim et al., 2009; Pece et al., 2010); p values represent the hypergeometric probability based on all 20,309 probes in the mouse array and 19,828 probes in the human arrays.

(C) Identification of genes unique to fMaSC and fSTR populations (Venn diagrams) and clustering of expression array data for these genes for fMaSC (f), fSTR (s), aMaSC (a), E15.5 mammary rudiments (b, buds), and lineage-depleted adult mammary epithelium (e) (heat maps).

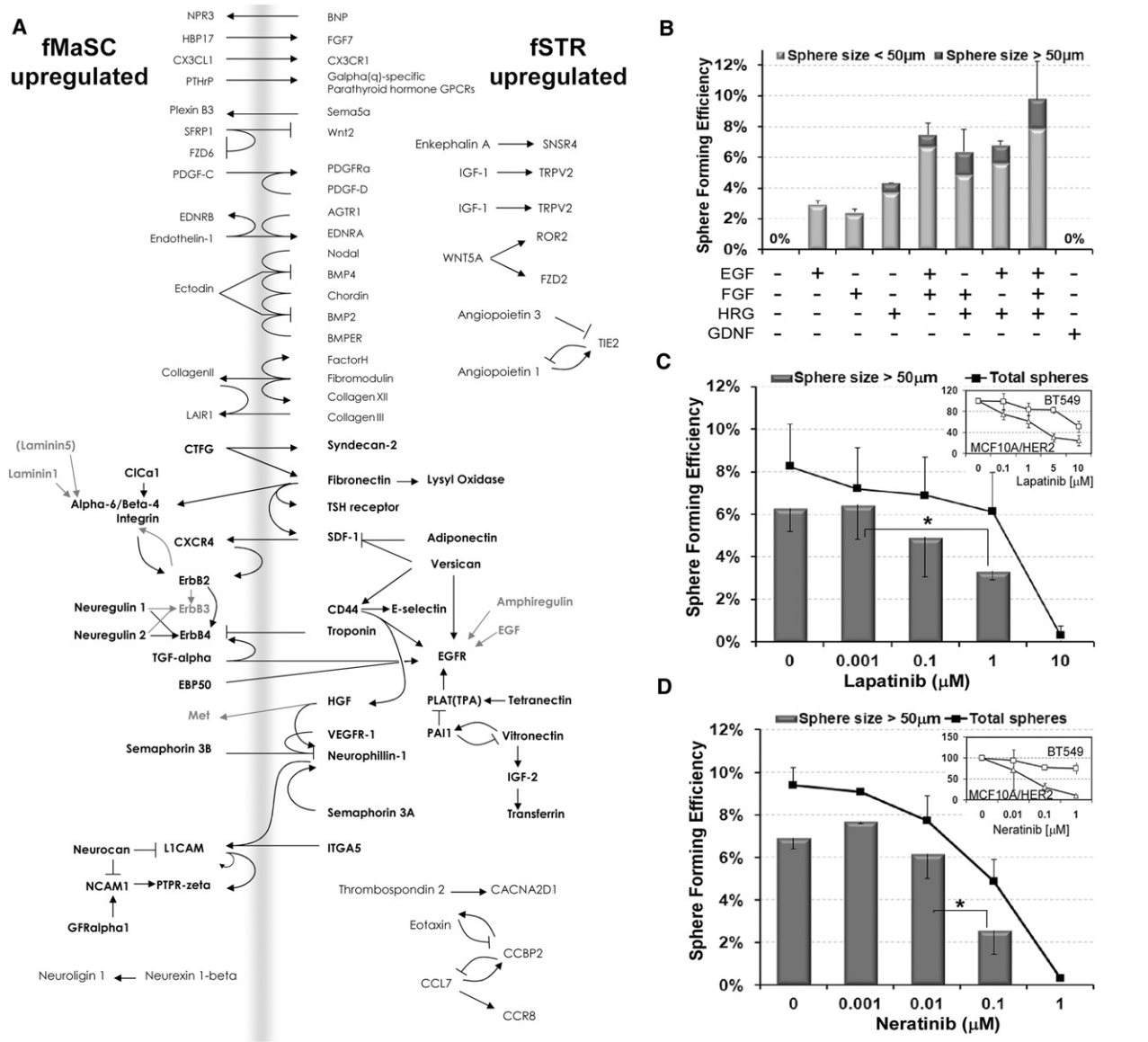

Figure 5. Prediction and Validation of Nonautonomous Signaling in fMaSC Function

(A) A model constructed from fetal gene signatures filtered for receptors and ligands with the GeneGo pathway analysis platform. The model illustrates candidate protein-protein interactions including receptor-ligand pairs expressed reciprocally in the fMaSC (left) and fSTR (right) populations. Additional gene products of interest predicted to interact with the network are also indicated (gray). The map suggests that ErbB signaling, among other pathways, may play a prominent role in fMaSC function.

(B) Quantification of fMaSC-derived spheres in the absence and presence of growth factors suggested by the model in (A).

(C) Quantification of fMaSC-derived sphere growth upon inhibition of ErbB1/2 signaling by either lapatinib or inhibition of ErbB1/2/4 signaling by neratinib. *$p < 0.05$, Student's t test.

(D) Dose-response curves to lapatinib and neratinib in resistant human BT549 and sensitive MCF10A/HER2 cell lines (Wang et al., 2006; Weigelt et al., 2010). All error bars indicate SD. See also Figure S5.

regimen (Paik et al., 2008). Our results show that fMaSCs, which would probably also be designated as ErbB2 negative with accepted clinical guidelines, are sensitive to ErbB pathway inhibitors. We speculate that tumors acquiring an fMaSC-like state will rely on ErbB pathway signaling and, therefore, be sensitive to ErbB antagonists despite being clinically designated as

(D) Gene ontology enrichment analysis of genes unique to the fMaSC and fSTR signatures. Each globe represents an ontological category and the size of the globe represents the number of genes in the category. Significantly enriched categories are color coded in red for fMaSC and blue for fSTR (Benjamini-Hochberg adjusted FDR = 5%). The organic layout algorithm used (Cytoscape) allows visualization of dense ontological data and the observation that many categories are enriched for each signature type. The most highly enriched categories are color coded in orange. The categories with the lowest p values and the gene names contributing to the most enriched "biological process" for each population are listed to the right. See also Figure S4 and Tables S4 and S5.

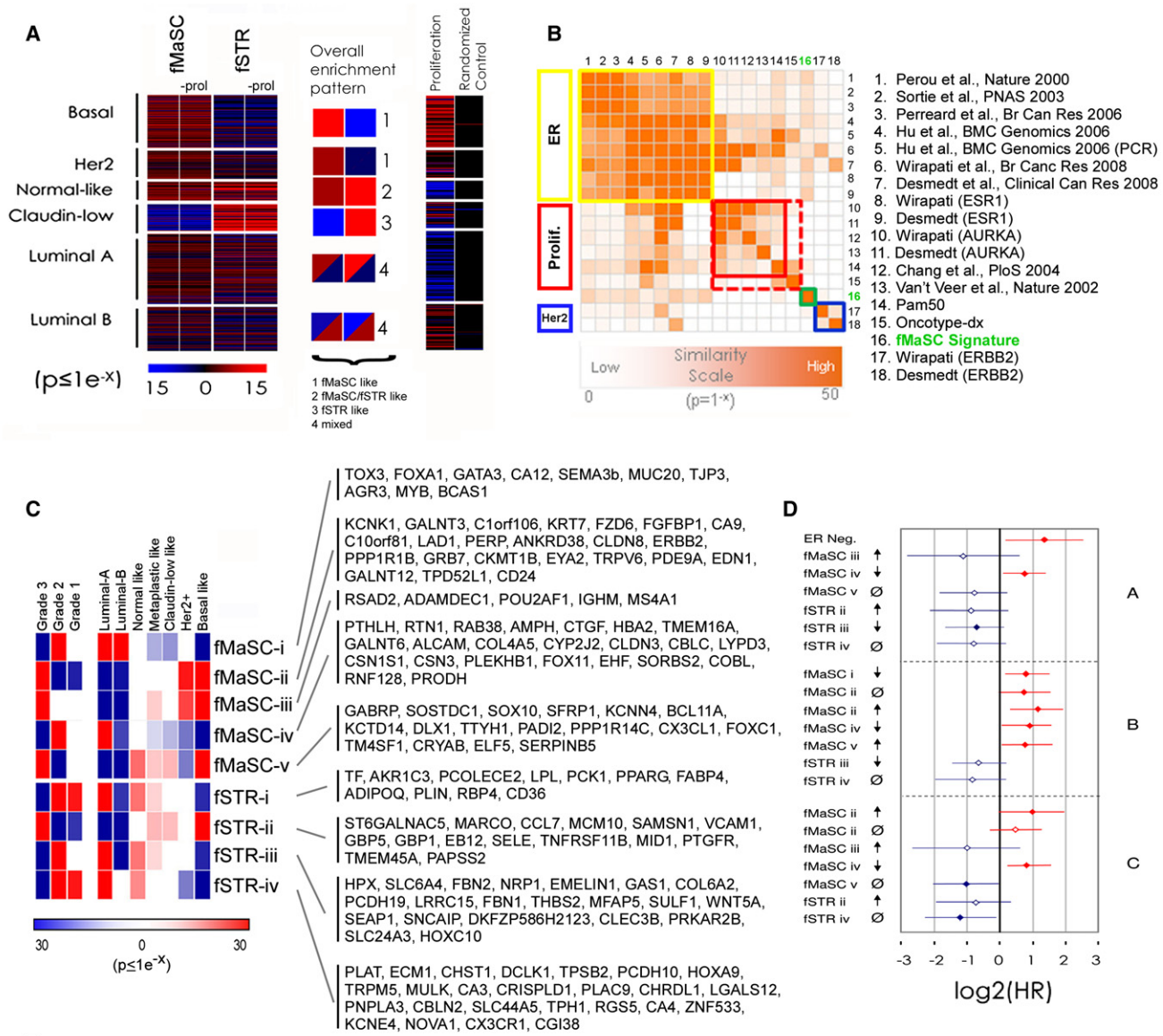

Figure 6. Fetal Mammary Gene Expression Patterns Provide Molecular Links to Human Breast Cancers

(A) Significant correlation between fMaSC and fSTR gene signatures and human breast cancers (n = 337) (Prat et al., 2010) are indicated by horizontal bars, each representing the gene expression profile from an individual tumor sample. Red bars indicate tumors enriched in fetal signature expression; blue bars indicate signature repression. Black bars indicate no significant correlation. Larger colored squares illustrate the trend for each intrinsic subtype. For comparison, a randomized signature of equivalent size and a proliferation signature (Ben-Porath et al., 2008) are shown.

(B) A comparison of several signatures and clinical metrics by significance of gene overlap. Most signatures are closely related and are significantly associated with ER (yellow box) or Proliferation (AURKA; red box) related signatures. Because of its size, the small OncotypeDX signature shows modest significance values for the proliferation group, although it includes several proliferation ER- and Her2-related genes. The fMaSC signature (green box and arrows) is relatively unique and shows no significant overlap with proliferation or ErbB2/Her2-related signatures (blue) and relatively low association with ER-related signatures.

(C) Significance of enrichment for subsignatures among diverse breast cancers in a large microarray compendium (n = 1,211) (Ben-Porath et al., 2008). Enrichments according to subtype and grade are indicated by colored squares that represent probabilities for the percentage of tumors enriched or repressed in each annotation group. Genes comprising each subsignature are listed.

(D) Subsignatures showing significance (◆, $p \leq 0.1$) or trends (◇, $p \leq 0.25$) in multivariate analysis are graphed for models including the following categorical clinical variables: A: ER status, grade, lymph-node status, tumor size; B: grade, lymph-node status and tumor size; C: ER status, lymph-node status and size

ErbB2 negative. The disproportionate representation of proliferation-, ER-, and Her2-related signaling in many existing prognostic signatures may mask less prominent yet critical signaling pathways that can be uncovered by studying normal developmental paradigms such as the fMaSC and fSTR states that are perturbed in cancer.

Links between embryogenesis and tumorigenesis were first proposed in 1838 by Müller as the stem cell origin of cancer and then extended by Durante and Conheim's hypothesis that elements remaining in an undifferentiated embryonic state or that reacquire characteristics of this state generate malignancies (Brewer et al., 2009; Sell, 2010). Subsequent descriptions of onco-fetal proteins, identification of embryonic stem cell genes, splice isoforms, microRNAs, and embryonic metabolism in cancer add credence to this concept (Brewer et al., 2009; Christofk et al., 2008; Powers and Mu, 2008; Sell, 2010). Our identification of a population of fMaSCs and associated stroma with gene expression signatures enriched in different types of breast cancer further support the importance of understanding both components and their interaction during cancer progression.

We suggest that cells resurrecting the programs that govern fetal tissue stem cells and fetal stroma may subsequently fuel tumor progression in the adult. This raises the question of how cells eliciting such programs arise during tumor progression. In some breast cancers, oncogenic lesions, such as loss of p53, may impart developmental plasticity, either directly or through reprogramming of tumor cells to more primitive states, including those resembling fMaSC or fSTR (Mizuno et al., 2010; Spike and Wahl, 2011). In this regard, the gene expression network we report involving both the fMaSCs and their associated stroma will provide a resource for generating new molecular hypotheses linking development and cancer, developing new diagnostic and prognostic metrics, and identifying candidate therapeutic targets.

EXPERIMENTAL PROCEDURES

Mice and Embryos

CD-1 and CB17-SCID were purchased from Charles River. Actin-eGFP mice were maintained on a CD-1 mixed background or pure C57BL/6J (Jackson Labs).

Cell Preparation

Adult mammary glands were dissociated according to the Stem Cell Technologies (SCT) protocol. For fetal mammary glands, collagenase/hyaluronidase digestion time was reduced to 90 min and the trypsin treatment was omitted.

Flow Cytometry

Single-cell suspensions were incubated with 4′,6-diamidino-2-phenylindole (DAPI) and the following antibodies: Fc receptor (2.4G), biotinylated CD31/CD45/TER119 cocktail, CD24-PE (M1/69), CD49f-FITC (all from SCT) and streptavidin-PerCPcy5.5 (BD Biosciences).

Mammary Transplantation

Mammary transplantation (Deome et al., 1959) was carried out with pulled-glass capillaries and mouth pipetting. Transplanted glands were evaluated 6–12 weeks postsurgery.

Immunofluorescence

Whole mounts, paraffin sections, OCT sections, or cytospins were stained with antibodies to: keratin 14 (AF-64, Covance, 1:1,000), keratin 8 (Troma-1, DSHB, 1:100), CD24 (M1/69, BD Biosciences, 1:1,000), CD49f (GoH3, BD Biosciences, 1:1,000), casein (a gift from G. Smith and D. Medina, 1:25), vimentin (AB5733, Chemicon, 1:1,000) and ErbB2 (29D8, Cell Signaling, 1:500).

3D, In Vitro Culture

For suspension mammosphere culture, freshly sorted cells were plated on ultralow-adherence plates (Corning) at 1000 cells/cm^2 in Epicult-B mouse media containing B-supplement, rhEGF, rhbFGF, heparin, and penicillin/streptomycin. For the 2% Matrigel culture, cells were plated on ultralow-adherence plates (Corning) at 1000cells/cm^2 in mammosphere media supplemented with 2% Matrigel (growth factor reduced, BD Biosciences). For the 100% Matrigel culture, freshly sorted cells were seeded on top of a 30 μl bed of Matrigel (growth factor reduced) in 2% Matrigel media. Vehicle (DMSO), lapatinib (LC Laboratories), neratinib (HKI-272, Pfizer) or FGFR inhibitor (PD173074, gift from the Verma lab, Salk Institute) were added at the indicated doses. For the clonal sphere culture, single cells were sorted into 96-well, low-adherence plates at a single cell per well density in 2% Matrigel media. For the eGFP$^+$ and eGFP$^-$ mixing experiments, The eGFP$^+$ and eGFP$^-$ fMaSC and fSTR populations were mixed in a 1:1 or 1:4 ratio. fMaSCs were seeded at low density on top of Matrigel (growth factor reduced) in 2% Matrigel media and fSTR cells were seeded at both low and high densities in mammosphere media.

Microarray and Bioinformatic Analysis

RNA was linearly T7-amplified, and gene expression was measured with a Nimblegen Array (12x135k MM9; Roche Nimblegen). The data are available at the gene expression omnibus at http://www.ncbi.nlm.nih.gov/ under accession GSE27027. Data were RMA normalized and processed with Excel, TIGR-MeV, Genomica, Cytoscape and MedCalc softwares, and the DAVID website. Differential expression was determined with SAM at FDR < 10% (Tusher et al., 2001). Detailed experimental and statistical methods accompany this manuscript as supplemental information.

ACCESSION NUMBERS

The gene expression omnibus accession number for the microarray expression data reported in this paper is GSE27027.

SUPPLEMENTAL INFORMATION

Supplemental Information include six figures and eight tables and can be found with this article online at doi:10.1016/j.stem.2011.12.018.

ACKNOWLEDGMENTS

We dedicate this work to Evelyn Lauder, visionary founder and inspirational leader of the Breast Cancer Research Foundation, and Corinne Mentzelopoulos for generously supporting the Salk Institute. We thank J.C. Izpisua Belmonte, T. Bonnefoix, G. Cunha, C. Eaves, P. Eirew, L. Ellies, P. Gray, J. Green, S. Kinkel, A. Legler, D. Medina, C.M. Perou, A. Prat, A. Rodrigues, B. Vonderhaar, and Wahl Lab members for invaluable advice; Pfizer for neratinib; and BCRF, DOD-BCRP, Susan G. Komen for the Cure, the G. Harold and Leila Y. Mathers Charitable Foundation, T32 training grants CA009523 (B.T.S.), GM07240 (D.D.E.), CA009370 (J.C.L.), and California Breast Cancer Research Program 15GB-0015 (D.D.E.) for funding; and National Cancer Institute 5P30CA014195 for core resource support.

Received: June 11, 2011
Revised: November 22, 2011
Accepted: December 22, 2011
Published online: February 2, 2012

(NKI295). A positive (or red) value indicates a poorer prognosis, while a negative (or blue) value indicates a better prognosis. The associated hazard for ER-negative tumors is shown in model A (versus fMaSC-i) for comparison. The following symbols are used: ↑ = subsignature enrichment; ↓ = subsignature repression; Ø = no significant signature enrichment and/or depletion. Error bars indicate 95th percentile CI.
(E) Biological functions associated with gene constituents of the subsignatures (gene set enrichment $p < 0.05$). See also Figures S6 and S7 and Tables S6–S8.

REFERENCES

Al-Hajj, M., Wicha, M.S., Benito-Hernandez, A., Morrison, S.J., and Clarke, M.F. (2003). Prospective identification of tumorigenic breast cancer cells. Proc. Natl. Acad. Sci. USA *100*, 3983–3988.

Anbazhagan, R., Osin, P.P., Bartkova, J., Nathan, B., Lane, E.B., and Gusterson, B.A. (1998). The development of epithelial phenotypes in the human fetal and infant breast. J. Pathol. *184*, 197–206.

Ben-Porath, I., Thomson, M.W., Carey, V.J., Ge, R., Bell, G.W., Regev, A., and Weinberg, R.A. (2008). An embryonic stem cell-like gene expression signature in poorly differentiated aggressive human tumors. Nat. Genet. *40*, 499–507.

Bonnefoix, T., Bonnefoix, P., Verdiel, P., and Sotto, J.J. (1996). Fitting limiting dilution experiments with generalized linear models results in a test of the single-hit Poisson assumption. J. Immunol. Methods *194*, 113–119.

Brewer, B.G., Mitchell, R.A., Harandi, A., and Eaton, J.W. (2009). Embryonic vaccines against cancer: An early history. Exp. Mol. Pathol. *86*, 192–197.

Britsch, S. (2007). The neuregulin-I/ErbB signaling system in development and disease. Adv. Anat. Embryol. Cell Biol. *190*, 1–65.

Chang, H.Y., Sneddon, J.B., Alizadeh, A.A., Sood, R., West, R.B., Montgomery, K., Chi, J.T., van de Rijn, M., Botstein, D., and Brown, P.O. (2004). Gene expression signature of fibroblast serum response predicts human cancer progression: Similarities between tumors and wounds. PLoS Biol. *2*, E7.

Christofk, H.R., Vander Heiden, M.G., Harris, M.H., Ramanathan, A., Gerszten, R.E., Wei, R., Fleming, M.D., Schreiber, S.L., and Cantley, L.C. (2008). The M2 splice isoform of pyruvate kinase is important for cancer metabolism and tumour growth. Nature *452*, 230–233.

Creighton, C.J., Li, X., Landis, M., Dixon, J.M., Neumeister, V.M., Sjolund, A., Rimm, D.L., Wong, H., Rodriguez, A., Herschkowitz, J.I., et al. (2009). Residual breast cancers after conventional therapy display mesenchymal as well as tumor-initiating features. Proc. Natl. Acad. Sci. USA *106*, 13820–13825.

Cunha, G.R., and Hom, Y.K. (1996). Role of mesenchymal-epithelial interactions in mammary gland development. J. Mammary Gland Biol. Neoplasia *1*, 21–35.

Deome, K.B., Faulkin, L.J., Jr., Bern, H.A., and Blair, P.B. (1959). Development of mammary tumors from hyperplastic alveolar nodules transplanted into gland-free mammary fat pads of female C3H mice. Cancer Res. *19*, 515–520.

Desmedt, C., Haibe-Kains, B., Wirapati, P., Buyse, M., Larsimont, D., Bontempi, G., Delorenzi, M., Piccart, M., and Sotiriou, C. (2008). Biological processes associated with breast cancer clinical outcome depend on the molecular subtypes. Clin. Cancer Res. *14*, 5158–5165.

Dontu, G., Al-Hajj, M., Abdallah, W.M., Clarke, M.F., and Wicha, M.S. (2003). Stem cells in normal breast development and breast cancer. Cell Prolif. *36* (*Suppl 1*), 59–72.

Fan, C., Oh, D.S., Wessels, L., Weigelt, B., Nuyten, D.S., Nobel, A.B., van't Veer, L.J., and Perou, C.M. (2006). Concordance among gene-expression-based predictors for breast cancer. N. Engl. J. Med. *355*, 560–569.

Fan, C., Prat, A., Parker, J.S., Liu, Y., Carey, L.A., Troester, M.A., and Perou, C.M. (2011). Building prognostic models for breast cancer patients using clinical variables and hundreds of gene expression signatures. BMC Med. Genomics *4*, 3.

Haibe-Kains, B., Desmedt, C., Piette, F., Buyse, M., Cardoso, F., Van't Veer, L., Piccart, M., Bontempi, G., and Sotiriou, C. (2008). Comparison of prognostic gene expression signatures for breast cancer. BMC Genomics *9*, 394.

Hanahan, D., and Weinberg, R.A. (2011). Hallmarks of cancer: The next generation. Cell *144*, 646–674.

Hay, E.D., and Zuk, A. (1995). Transformations between epithelium and mesenchyme: Normal, pathological, and experimentally induced. Am. J. Kidney Dis. *26*, 678–690.

Hendrix, M.J., Seftor, E.A., Seftor, R.E., and Trevor, K.T. (1997). Experimental co-expression of vimentin and keratin intermediate filaments in human breast cancer cells results in phenotypic interconversion and increased invasive behavior. Am. J. Pathol. *150*, 483–495.

Hennessy, B.T., Gonzalez-Angulo, A.M., Stemke-Hale, K., Gilcrease, M.Z., Krishnamurthy, S., Lee, J.S., Fridlyand, J., Sahin, A., Agarwal, R., Joy, C., et al. (2009). Characterization of a naturally occurring breast cancer subset enriched in epithelial-to-mesenchymal transition and stem cell characteristics. Cancer Res. *69*, 4116–4124.

Herschkowitz, J.I., Simin, K., Weigman, V.J., Mikaelian, I., Usary, J., Hu, Z., Rasmussen, K.E., Jones, L.P., Assefnia, S., Chandrasekharan, S., et al. (2007). Identification of conserved gene expression features between murine mammary carcinoma models and human breast tumors. Genome Biol. *8*, R76.

Howard, B., and Ashworth, A. (2006). Signalling pathways implicated in early mammary gland morphogenesis and breast cancer. PLoS Genet. *2*, e112.

Hu, Y., and Smyth, G.K. (2009). ELDA: Extreme limiting dilution analysis for comparing depleted and enriched populations in stem cell and other assays. J. Immunol. Methods *347*, 70–78.

Jackson-Fisher, A.J., Bellinger, G., Ramabhadran, R., Morris, J.K., Lee, K.F., and Stern, D.F. (2004). ErbB2 is required for ductal morphogenesis of the mammary gland. Proc. Natl. Acad. Sci. USA *101*, 17138–17143.

Jackson-Fisher, A.J., Bellinger, G., Breindel, J.L., Tavassoli, F.A., Booth, C.J., Duong, J.K., and Stern, D.F. (2008). ErbB3 is required for ductal morphogenesis in the mouse mammary gland. Breast Cancer Res. *10*, R96.

Jacobs, T.W., Gown, A.M., Yaziji, H., Barnes, M.J., and Schnitt, S.J. (1999). Specificity of HercepTest in determining HER-2/neu status of breast cancers using the United States Food and Drug Administration-approved scoring system. J. Clin. Oncol. *17*, 1983–1987.

Jones, D.L., and Wagers, A.J. (2008). No place like home: Anatomy and function of the stem cell niche. Nat. Rev. Mol. Cell Biol. *9*, 11–21.

Karaman, M.W., Herrgard, S., Treiber, D.K., Gallant, P., Atteridge, C.E., Campbell, B.T., Chan, K.W., Ciceri, P., Davis, M.I., Edeen, P.T., et al. (2008). A quantitative analysis of kinase inhibitor selectivity. Nat. Biotechnol. *26*, 127–132.

Kendrick, H., Regan, J.L., Magnay, F.A., Grigoriadis, A., Mitsopoulos, C., Zvelebil, M., and Smalley, M.J. (2008). Transcriptome analysis of mammary epithelial subpopulations identifies novel determinants of lineage commitment and cell fate. BMC Genomics *9*, 591.

Kikuchi, A., Yamamoto, H., Sato, A., and Matsumoto, S. (2012). Wnt5a: Its signalling, functions and implication in diseases. Acta Physiol. (Oxf.) *204*, 17–33.

Korkaya, H., and Wicha, M.S. (2009). HER-2, notch, and breast cancer stem cells: Targeting an axis of evil. Clin. Cancer Res. *15*, 1845–1847.

Lim, E., Vaillant, F., Wu, D., Forrest, N.C., Pal, B., Hart, A.H., Asselin-Labat, M.L., Gyorki, D.E., Ward, T., Partanen, A., et al; kConFab. (2009). Aberrant luminal progenitors as the candidate target population for basal tumor development in BRCA1 mutation carriers. Nat. Med. *15*, 907–913.

Lim, E., Wu, D., Pal, B., Bouras, T., Asselin-Labat, M.-L., Vaillant, F., Yagita, H., Lindeman, G.J., Smyth, G.K., and Visvader, J.E. (2010). Transcriptome analyses of mouse and human mammary cell subpopulations reveal multiple conserved genes and pathways. Breast Cancer Res. *12*, R21.

Livasy, C.A., Reading, F.C., Moore, D.T., Boggess, J.F., and Lininger, R.A. (2006). EGFR expression and HER2/neu overexpression/amplification in endometrial carcinosarcoma. Gynecol. Oncol. *100*, 101–106.

Mani, S.A., Guo, W., Liao, M.J., Eaton, E.N., Ayyanan, A., Zhou, A.Y., Brooks, M., Reinhard, F., Zhang, C.C., Shipitsin, M., et al. (2008). The epithelial-mesenchymal transition generates cells with properties of stem cells. Cell *133*, 704–715.

Mizuno, H., Spike, B.T., Wahl, G.M., and Levine, A.J. (2010). Inactivation of p53 in breast cancers correlates with stem cell transcriptional signatures. Proc. Natl. Acad. Sci. USA *107*, 22745–22750.

Mørk, C., van Deurs, B., and Petersen, O.W. (1990). Regulation of vimentin expression in cultured human mammary epithelial cells. Differentiation *43*, 146–156.

Paik, S., Tang, G., Shak, S., Kim, C., Baker, J., Kim, W., Cronin, M., Baehner, F.L., Watson, D., Bryant, J., et al. (2006). Gene expression and benefit of chemotherapy in women with node-negative, estrogen receptor-positive breast cancer. J. Clin. Oncol. *24*, 3726–3734.

Paik, S., Kim, C., and Wolmark, N. (2008). HER2 status and benefit from adjuvant trastuzumab in breast cancer. N. Engl. J. Med. *358*, 1409–1411.

Pal, S.K., Childs, B.H., and Pegram, M. (2011). Triple negative breast cancer: Unmet medical needs. Breast Cancer Res. Treat. *125*, 627–636.

Pece, S., Tosoni, D., Confalonieri, S., Mazzarol, G., Vecchi, M., Ronzoni, S., Bernard, L., Viale, G., Pelicci, P.G., and Di Fiore, P.P. (2010). Biological and molecular heterogeneity of breast cancers correlates with their cancer stem cell content. Cell *140*, 62–73.

Perou, C.M., Sørlie, T., Eisen, M.B., van de Rijn, M., Jeffrey, S.S., Rees, C.A., Pollack, J.R., Ross, D.T., Johnsen, H., Akslen, L.A., et al. (2000). Molecular portraits of human breast tumours. Nature *406*, 747–752.

Perou, C.M., Parker, J.S., Prat, A., Ellis, M.J., and Bernard, P.S. (2010). Clinical implementation of the intrinsic subtypes of breast cancer. Lancet Oncol. *11*, 718–719, author reply 720–721.

Petersen, O.W., and Polyak, K. (2010). Stem cells in the human breast. Cold Spring Harb Perspect Biol. *2*, a003160.

Powers, S., and Mu, D. (2008). Genetic similarities between organogenesis and tumorigenesis of the lung. Cell Cycle *7*, 200–204.

Prat, A., and Perou, C.M. (2011). Deconstructing the molecular portraits of breast cancer. Mol. Oncol. *5*, 5–23.

Prat, A., Parker, J.S., Karginova, O., Fan, C., Livasy, C., Herschkowitz, J.I., He, X., and Perou, C.M. (2010). Phenotypic and molecular characterization of the claudin-low intrinsic subtype of breast cancer. Breast Cancer Res. *12*, R68.

Rabindran, S.K., Discafani, C.M., Rosfjord, E.C., Baxter, M., Floyd, M.B., Golas, J., Hallett, W.A., Johnson, B.D., Nilakantan, R., Overbeek, E., et al. (2004). Antitumor activity of HKI-272, an orally active, irreversible inhibitor of the HER-2 tyrosine kinase. Cancer Res. *64*, 3958–3965.

Raouf, A., Zhao, Y., To, K., Stingl, J., Delaney, A., Barbara, M., Iscove, N., Jones, S., McKinney, S., Emerman, J., et al. (2008). Transcriptome analysis of the normal human mammary cell commitment and differentiation process. Cell Stem Cell *3*, 109–118.

Rody, A., Karn, T., Liedtke, C., Pusztai, L., Ruckhaeberle, E., Hanker, L., Gaetje, R., Solbach, C., Ahr, A., Metzler, D., et al. (2011). A clinically relevant gene signature in triple negative and basal-like breast cancer. Breast Cancer Res. *13*, R97.

Rusnak, D.W., Lackey, K., Affleck, K., Wood, E.R., Alligood, K.J., Rhodes, N., Keith, B.R., Murray, D.M., Knight, W.B., Mullin, R.J., and Gilmer, T.M. (2001). The effects of the novel, reversible epidermal growth factor receptor/ErbB-2 tyrosine kinase inhibitor, GW2016, on the growth of human normal and tumor-derived cell lines in vitro and in vivo. Mol. Cancer Ther. *1*, 85–94.

Sakakura, T., Nishizuka, Y., and Dawe, C.J. (1979). Capacity of mammary fat pads of adult C3H/HeMs mice to interact morphogenetically with fetal mammary epithelium. J. Natl. Cancer Inst. *63*, 733–736.

Sell, S. (2010). On the stem cell origin of cancer. Am. J. Pathol. *176*, 2584–494.

Shackleton, M., Vaillant, F., Simpson, K.J., Stingl, J., Smyth, G.K., Asselin-Labat, M.L., Wu, L., Lindeman, G.J., and Visvader, J.E. (2006). Generation of a functional mammary gland from a single stem cell. Nature *439*, 84–88.

Sørlie, T., Perou, C.M., Tibshirani, R., Aas, T., Geisler, S., Johnsen, H., Hastie, T., Eisen, M.B., van de Rijn, M., Jeffrey, S.S., et al. (2001). Gene expression patterns of breast carcinomas distinguish tumor subclasses with clinical implications. Proc. Natl. Acad. Sci. USA *98*, 10869–10874.

Sotiriou, C., and Piccart, M.J. (2007). Taking gene-expression profiling to the clinic: When will molecular signatures become relevant to patient care? Nat. Rev. Cancer *7*, 545–553.

Spike, B.T., and Wahl, G.M. (2011). p53, Stem Cells, and Reprogramming: Tumor Suppression beyond Guarding the Genome. Genes Cancer *2*, 404–419.

Spradling, A., Drummond-Barbosa, D., and Kai, T. (2001). Stem cells find their niche. Nature *414*, 98–104.

Stingl, J., Eirew, P., Ricketson, I., Shackleton, M., Vaillant, F., Choi, D., Li, H.I., and Eaves, C.J. (2006). Purification and unique properties of mammary epithelial stem cells. Nature *439*, 993–997.

Strizzi, L., Hardy, K.M., Seftor, E.A., Costa, F.F., Kirschmann, D.A., Seftor, R.E., Postovit, L.M., and Hendrix, M.J. (2009). Development and cancer: At the crossroads of Nodal and Notch signaling. Cancer Res. *69*, 7131–7134.

Sun, P., Yuan, Y., Li, A., Li, B., and Dai, X. (2010). Cytokeratin expression during mouse embryonic and early postnatal mammary gland development. Histochem. Cell Biol. *133*, 213–221.

Thiery, J.P., and Sleeman, J.P. (2006). Complex networks orchestrate epithelial-mesenchymal transitions. Nat. Rev. Mol. Cell Biol. *7*, 131–142.

Thomas, P.A., Kirschmann, D.A., Cerhan, J.R., Folberg, R., Seftor, E.A., Sellers, T.A., and Hendrix, M.J. (1999). Association between keratin and vimentin expression, malignant phenotype, and survival in postmenopausal breast cancer patients. Clin. Cancer Res. *5*, 2698–2703.

Tidcombe, H., Jackson-Fisher, A., Mathers, K., Stern, D.F., Gassmann, M., and Golding, J.P. (2003). Neural and mammary gland defects in ErbB4 knockout mice genetically rescued from embryonic lethality. Proc. Natl. Acad. Sci. USA *100*, 8281–8286.

Tusher, V.G., Tibshirani, R., and Chu, G. (2001). Significance analysis of microarrays applied to the ionizing radiation response. Proc. Natl. Acad. Sci. USA *98*, 5116–5121.

van de Vijver, M.J., He, Y.D., van't Veer, L.J., Dai, H., Hart, A.A., Voskuil, D.W., Schreiber, G.J., Peterse, J.L., Roberts, C., Marton, M.J., et al. (2002). A gene-expression signature as a predictor of survival in breast cancer. N. Engl. J. Med. *347*, 1999–2009.

Van Keymeulen, A., Rocha, A.S., Ousset, M., Beck, B., Bouvencourt, G., Rock, J., Sharma, N., Dekoninck, S., and Blanpain, C. (2011). Distinct stem cells contribute to mammary gland development and maintenance. Nature *479*, 189–193.

van 't Veer, L.J., Dai, H., van de Vijver, M.J., He, Y.D., Hart, A.A., Mao, M., Peterse, H.L., van der Kooy, K., Marton, M.J., Witteveen, A.T., et al. (2002). Gene expression profiling predicts clinical outcome of breast cancer. Nature *415*, 530–536.

Veltmaat, J.M., Mailleux, A.A., Thiery, J.P., and Bellusci, S. (2003). Mouse embryonic mammogenesis as a model for the molecular regulation of pattern formation. Differentiation *71*, 1–17.

Wang, S.E., Narasanna, A., Perez-Torres, M., Xiang, B., Wu, F.Y., Yang, S., Carpenter, G., Gazdar, A.F., Muthuswamy, S.K., and Arteaga, C.L. (2006). HER2 kinase domain mutation results in constitutive phosphorylation and activation of HER2 and EGFR and resistance to EGFR tyrosine kinase inhibitors. Cancer Cell *10*, 25–38.

Wansbury, O., Mackay, A., Kogata, N., Mitsopoulos, C., Kendrick, H., Davidson, K., Ruhrberg, C., Reis-Filho, J.S., Smalley, M.J., Zvelebil, M., and Howard, B.A. (2011). Transcriptome analysis of embryonic mammary cells reveals insights into mammary lineage establishment. Breast Cancer Res. *13*, R79.

Weigelt, B., Lo, A.T., Park, C.C., Gray, J.W., and Bissell, M.J. (2010). HER2 signaling pathway activation and response of breast cancer cells to HER2-targeting agents is dependent strongly on the 3D microenvironment. Breast Cancer Res. Treat. *122*, 35–43.

Wirapati, P., Sotiriou, C., Kunkel, S., Farmer, P., Pradervand, S., Haibe-Kains, B., Desmedt, C., Ignatiadis, M., Sengstag, T., Schütz, F., et al. (2008). Meta-analysis of gene expression profiles in breast cancer: Toward a unified understanding of breast cancer subtyping and prognosis signatures. Breast Cancer Res. *10*, R65.

Zeng, Y.A., and Nusse, R. (2010). Wnt proteins are self-renewal factors for mammary stem cells and promote their long-term expansion in culture. Cell Stem Cell *6*, 568–577.

Supplemental Information:

Cell Stem Cell, Volume *10*
Supplemental Data

A Mammary Stem Cell Population Identified and Characterized in Late Embryogenesis Reveals Similarities to Human Breast Cancer

Benjamin T. Spike, Dannielle D. Engle, Jennifer C. Lin, Samantha K. Cheung, Justin La, and Geoffrey M. Wahl

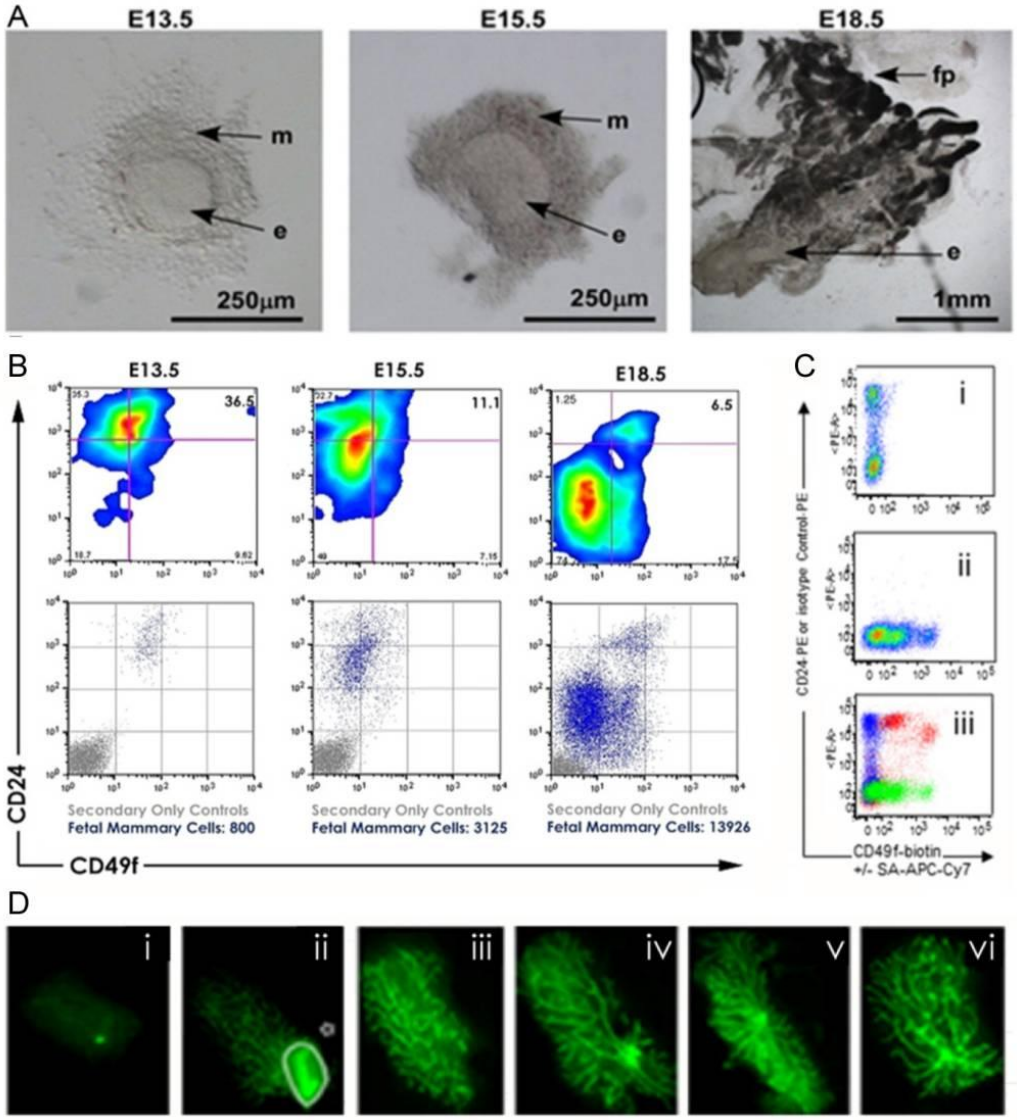

Figure S1. Related to Figure 1. Additional phenotypic and functional evaluation of fetal mammary rudiments. **(A)** Brightfield images of dissected intact rudiments from E13.5, E15.5 and E18.5 indicating contribution by: m=mesenchyme, e=epithelium, fp=fat pad identified according to morphology. **(B)** FACS density plots showing population centers of mammary rudiment cells according to their expression of CD24 and CD49f at E13.5, E15.5 and E18.5 (upper panels). FACS dot plots showing the distribution of cells expressing CD24 and CD49f in the LIN^- mammary rudiments (blue) relative to unlabeled controls (gray) (lower panels). **(C)** Typical compensation controls for FACS labeling using single color labeling (density plots and green and blue plots) with an overlaid fully labeled adult sample (red). **(D)** Intact fetal pieces including mammary epithelium and associated mesenchyme (from actin-eGFP+ donors) can repopulate cleared fat pads with mammary epithelial outgrowths *in vivo*. Transplanting intact pieces from E10.5 did not result in mammary gland reconstitution (i), while pieces with mammary epithelium plus associated mesenchyme from developmental stage E11.5 (ii), E12.5 (iii), E13.5 (iv), E15.5 (v), and E18.5 (vi) resulted in reconstitution of mammary gland and sometimes the growth of hair (ii). The star symbol (ii) indicates levels adjusted separately for outlined area due to overexposure.

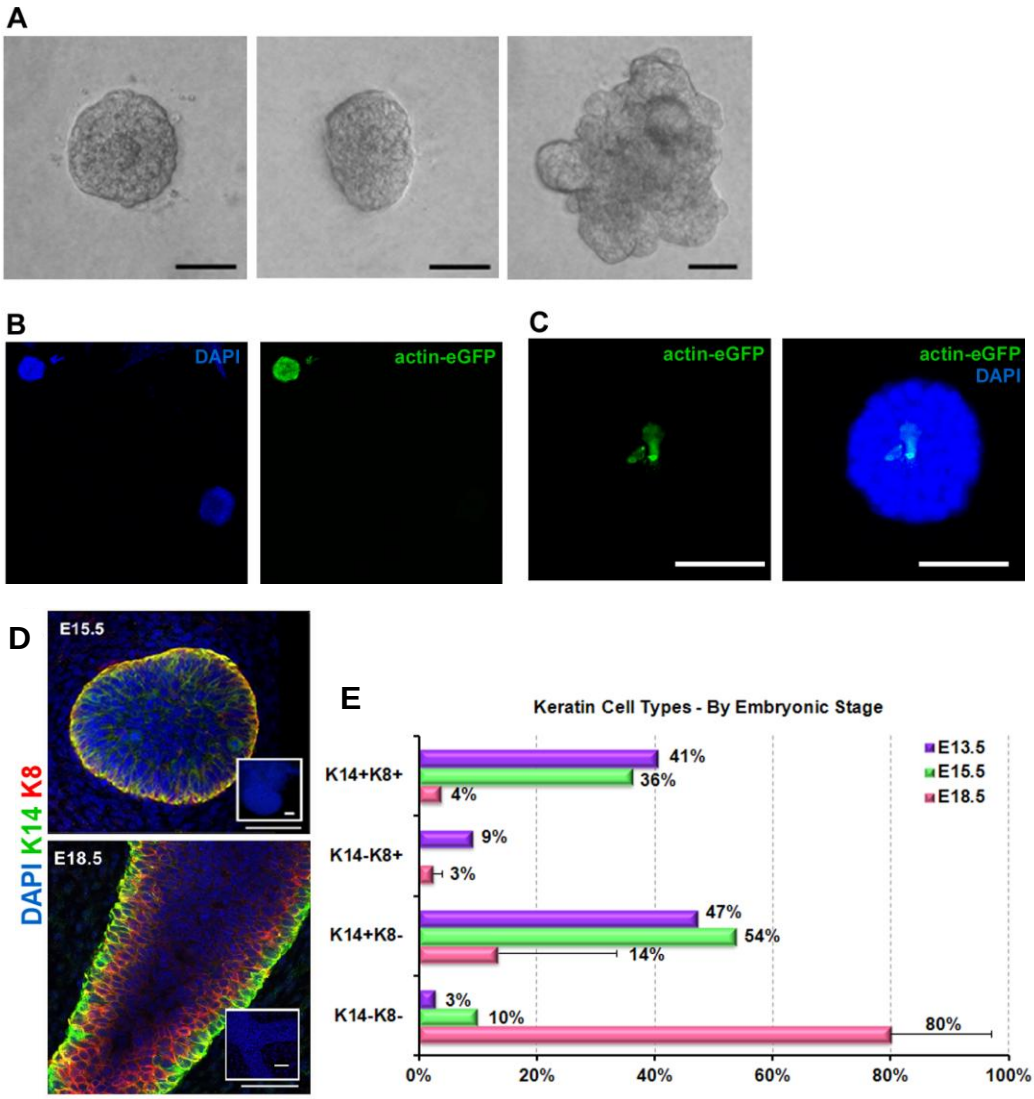

Figure S2. Related to Figure 2. Individual cells from the fMaSC population generate clonal primary spheres. **(A)** Brightfield images of primary spheres generated from single cells cultured in individual wells of 96 well plates (n=3, at least 3 96-well plates per experiment, sphere forming efficiency = 10.7 ± 1.5%). **(B and C)** Cells from the fMaSC populations were independently prepared from actin-eGFP mice (mixed strain, CD1/C57BL6) and WT mice (CD1 strain), mixed in a 1:1 ratio (B) and a 4:1 ratio (C), and seeded on top of Matrigel. In this experiment, 207 spheres were a single color and one sphere was chimeric (shown in C). **(D)** Confocal immunofluorescence analysis of E15.5 and E18.5 mammary rudiments showing cells expressing K8 (red), K14 (green), both and neither with nuclear counterstain DAPI (blue). Insets, secondary antibody only. **(E)** Percentage summary of K14 and K8 positive and negative cells in E13.5, E15.5 and E18.5 bulk mammary cell suspensions evaluated by immunofluorescence on cytospins of freshly isolated cells. Error bars, standard deviation. Scale bar, 50μm.

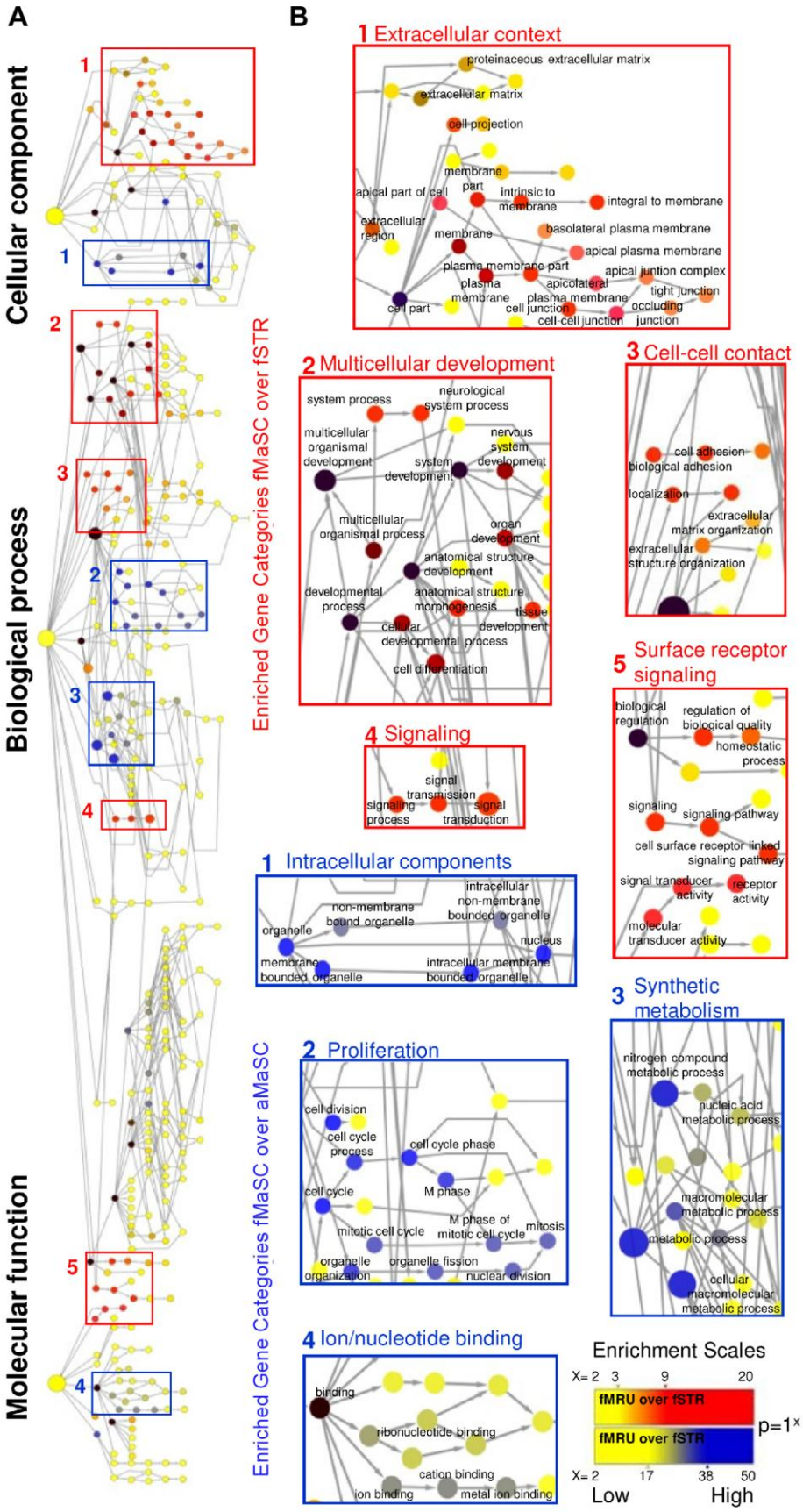

Figure S3. Related to Figure 3. Ontological enrichments for fMaSC and fSTR signatures. **(A)** Ontological categories with representation from fetal signature genes are grouped by molecular function, biological process or cellular component categories. Node size indicates the relative size of the category in the database. The significance of specific category enrichments for the fMaSC signature (red) and the genes overexpressed in fMaSCs relative to aMaSCs (blue) are indicated by the shading of the nodes. Groups of categories predominantly associated with fMaSC and fMaSC/aMaSC are indicated by the colored boxes. **(B)** Detail of fMaSC and fMaSC/aMaSC categorical groups identified in A. The fMaSC signature is associated with paracrine signaling and distinguishable from aMaSC by categories including proliferation and synthetic metabolism.

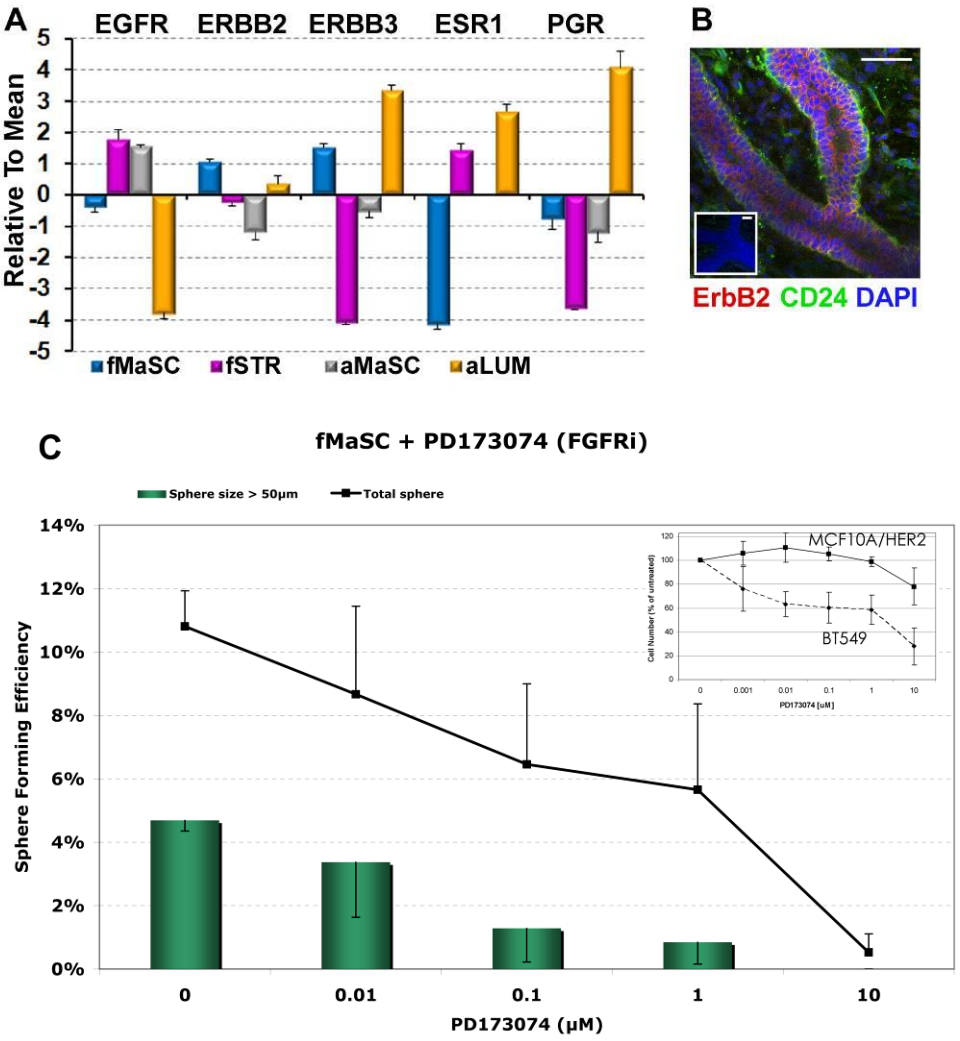

Figure S4. Expression of ErbB family members and hormone receptors and sensitivity of fMaSC derived sphere growth to FGFR inhibition. Related to Figure 5. **(A)** qRT-PCR analysis of the ErbB family receptors, Estrogen receptors, and Progesterone receptors in fMaSC, fSTR, aMaSC, and adult luminal (aLUM) cells. **(B)** Confocal immunofluorescence analysis of an E18.5 mammary rudiment showing cells expressing ErbB2 and CD24. Inset, secondary antibody control. Scale bar, 50µm. **(C)** E18.5 dissociated rudiments were sorted to obtain individual Lin-CD24^{high}CD49f^{high} cells (fMaSCs). fMaSCs were plated at clonal density and spheres were grown as in Figure 6. Cultures were treated with the FGFR inhibitor PD173074 at the concentrations indicated or with vehicle (DMSO). Spheres were grown for 6 days, counted and then tallied according to size. Error bars, standard deviation.

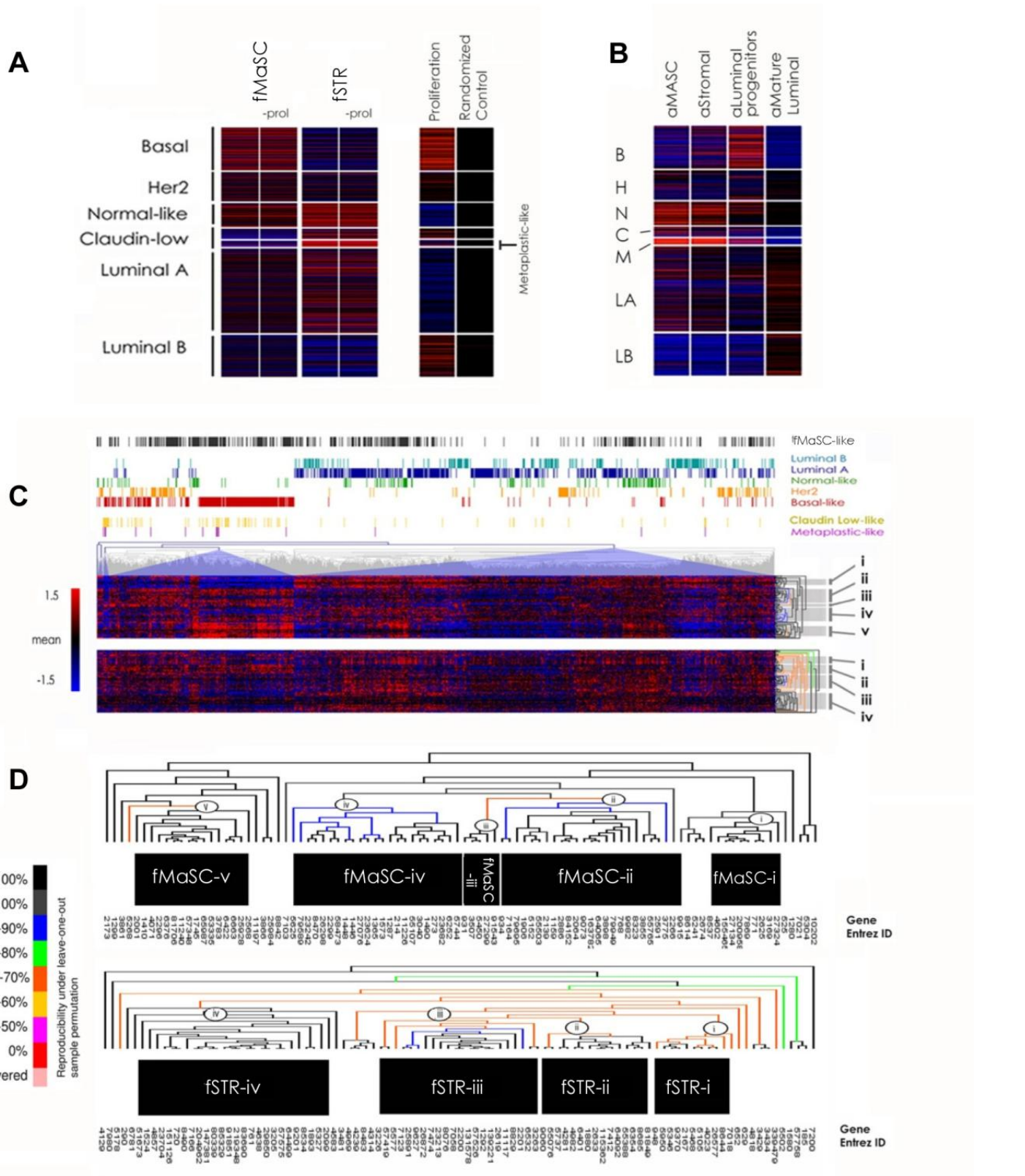
A
fMaSC
-prol
fSTR
-prol
Proliferation
Randomized Control
Basal
Her2
Normal-like
Claudin-low
Luminal A
Luminal B
Metaplastic-like
B
aMASC
aStromal
aLuminal progenitors
aMature Luminal
B
H
N
C
M
LA
LB
C
fMaSC-like
Luminal B
Luminal A
Normal-like
Her2
Basal-like
Claudin Low-like
Metaplastic-like
1.5
mean
-1.5
i
ii
iii
iv
v
i
ii
iii
iv
D
fMaSC-v
fMaSC-iv
fMaSC -iii
fMaSC-ii
fMaSC-i
Gene Entrez ID
100%
90-100%
80-90%
70-80%
60-70%
50-60%
0-50%
0%
unrecovered
Reproducibility under leave-one-out sample permutation
fSTR-iv
fSTR-iii
fSTR-ii
fSTR-i
Gene Entrez ID

Figure S5. Related to Figure 6. Signature enrichment as in Figure 6 and selection of coordinately expressed fetal subsignatures in an independent breast cancer microarray compendium (Ben-Porath et al., 2008). **(A)** Gene set enrichment in a breast cancer compendium consisting of over 1,200 samples compiled by Ben-Porath et al. showing patterns of enrichment highly similar to those observed in the UNC compendium in Figure 6A. The subtraction of genes from the proliferation signature (Prol-) reported in Ben-Porath et al. indicates a negligible effect of proliferation signature genes on fetal signature enrichment among breast tumors. **(B)** Previously designated adult MaSC, luminal progenitor, mature luminal and stromal signatures (Lim et al., 2010) enrichment patterns. aMaSC and aStromal signatures show enrichment patterns in tumors that are very similar to those observed for the fSTR population rather than the fMaSC population. **(C)** Hierarchical clustering of the 96 most highly variable fMaSC genes (upper heat map) shows fetal gene signature expression to be modular in human breast cancers. Intrinsic subtype designation and overall fMaSC enrichment are indicated by colored vertical bars. The lower, fSTR heat map is ordered according to hierarchical clustering of samples in the upper fMaSC heat map. **(D)** Detail of hierarchical gene cluster analysis of the fMaSC and fSTR signature genes. Hierarchical gene clusters from the 96 most variably expressed fMaSC and fSTR signature genes were analyzed by Leave-One-Out (jackknifing) permutation analysis (100 permutations) to indicate relative stability of coordinate expression. The gene clusters analyzed in Figure 6 in the manuscript are indicated in black boxes and the entrez ID's for genes corresponding to each branch in the dendrogram are indicated.

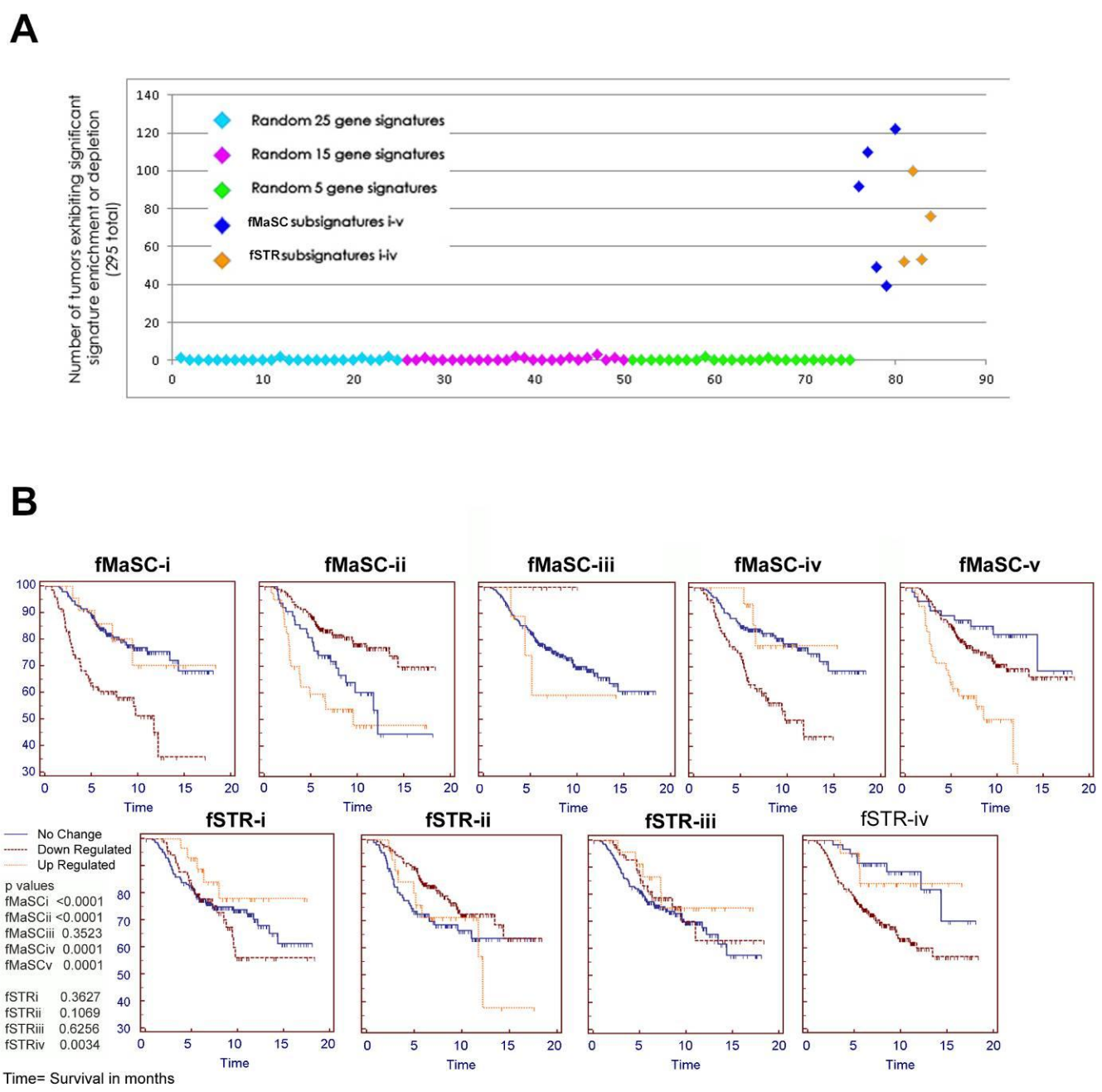

Figure S6. Related to Figure 6. **(A)** 25 random signatures of various sizes fail to exhibit significant enrichment in breast cancers. The random signatures comprising of 5, 15 or 25 genes were generated using Excel random number generator and the list of genes present on the array. These random signatures were tested individually for enrichment among tumors of the compendium using the same threshold as in Figure 6. The five fMaSC gene sets and fSTR gene sets were analyzed in parallel. The number of significantly enriched or depleted tumors is reported for each signature. Random signatures did not give rise to a sufficient number of significant enrichments or depletions for tumor classification and subsequent multivariate analyses. **(B)** Kaplan-Meier survival analysis using each of the fetal mammary subsignatures on the NKI295 breast cancer data set.

Supplemental Tables

Table S1. Related to Table 1. Limiting dilution mammary transplantation analyses of freshly dissociated, bulk or fractionated mammary cells.

Bulk mammary cells	Cells injected per fat pad	Repopulated fat pad #	
		No Matrigel	co-injected with Matrigel
E13.5	25	N.D.	0/2
	100	0/4	0/8
	1000	0/4	2/6
	10000	0/11	4/9
	MaSC freq (95% CI)	**<1/40,000**	**1/12,000 (1/5000 - 1/30,000)**
	p Value		0.2
* E15.5	10	N.D.	0/4
	100	N.D.	0/11
	500	0/5	4/9
	1000	0/10	2/7
	MaSC freq (95% CI)	**<1/4,000**	**1/1,800 (1/800-1/4,000)**
	p Value		0.9
* E16	50	N.D.	0/6
	100	N.D.	0/6
	500	N.D.	1/6
	1000	N.D.	1/6
	MaSC freq (95% CI)		**1/4,600† (1/1,000 - 1/18,000)**
	p Value		0.8
* E16.5	50	N.D.	2/3
	100	N.D.	3/9
	1000	N.D.	6/6
	MaSC freq (95% CI)		**1/200 (1/70 - 1/400)**
	p Value		0.68

p values > 0.05 indicate the data are consistent with a single-hit Poisson model.
† Rough MaSC frequency estimate (see Statistical Analyses under Methods for detail).
N.D.= not determined.
* $p < 0.001$, pairwise group difference.

Table S1 continued.

Bulk mammary cells	Cells injected per fat pad	Repopulated fat pad #	
		No Matrigel	co-injected with Matrigel
E18.5	10	N.D.	3/15
	20	N.D.	2/11
	25	N.D.	10/27
	50	0/6	18/30
	100	1/5	13/17
	1000	5/8	12/12
	2000	4/4	N.D.
	MaSC freq (95% CI)	**1/830 (1/400 - 1/1,600)**	**1/60 (1/40 - 1/80)**
	p Value	0.8 *	0.7
Adult	10	N.D.	0/10
	100	0/11	2/9
	500	N.D.	8/9
	1,000	2/17	8/8
	10,000	2/11	2/2
	20,000	N.D.	4/4
	MaSC freq (95% CI)	**1/30,000† (1/11,000-1/80,000)**	**1/300 (1/150 - 1/500)**
	p Value	0.2	0.2
Fractionated mammary cells		Repopulated fat pad #	
E18.5 fetal MaSC population ($CD24^{high}CD49f^{high}$)	5	N.D.	3/17
	10	N.D.	11/16
	20	1/10	14/20
	25	N.D.	12/14
	50	1/5	4/4
	100	0/4	4/4
	MaSC freq (95% CI)	**1/400† (1/100 - 1/1,700)**	**1/14 (1/10 - 1/18)**
	p Value	0.2	0.7
E18.5 fSTR population ($CD24^{med/low/neg}$)	50-300	0/11 *	0/9
	1000-3000	0/8	0/9
	MaSC freq (95% CI)	**<1/9,000**	**<1/5,000**
	p Value		
Adult MaSC population ($CD24^{med}CD49f^{high}$)	10	0/6	1/6
	50	1/6	4/6
	100	1/7	6/7
	1000	1/2	2/2
	MaSC freq (95% CI)	**1/800† (1/200 - 1/2,700)**	**1/50 (1/30 - 1/100)**
	p Value	0.4	0.98

p values > 0.05 indicate the data are consistent with a single-hit Poisson model.
† Rough MaSC frequency estimate (see Statistical Analyses under Methods for detail).
N.D.= not determined. * $p < 0.001$, pairwise group difference.

Table S2. Related to Table 1. Transplant efficiency from intact Actin-eGFP+ fetal mammary rudiments.

Fetal stage (intact pieces, actin-eGFP+)	Repopulated fat pad	Total fat pad transplanted	Transplant efficiency	Engraftment
E10.5	0	9	0	100%
E11.5	3	24	13%	100%
E12.5	5	7	70%	100%
E13.5	8	11	72%	N.D.
E15.5	10	10	100%	N.D.
E18.5	11	12	92%	N.D.

Engraftment = successful donor tissue implantation determined by visualization of GFP-expressing tissues in non-GFP expressing fat pads.
N.D. = not determined.

Table S3. Related to Table 1. Limiting dilution mammary transplantation analyses of fractionated adult and fetal mammary cells using syngeneic recipients.

Fractionated mammary cells	Cells injected per fat pad	Repopulated fat pad	
		No Matrigel	co-injected with Matrigel
E18.5 fMaSC population ($CD24^{high}CD49f^{high}$)	10	N.D.	7/10
	60	N.D.	10/10
	MaSC freq (95% CI)		**1/8** (1/4-1/18)
	p Value		
Adult MaSC population ($CD24^{med}CD49f^{high}$)	20	4/7	N.D.
	50	4/6	N.D.
	100	4/6	N.D.
	MaSC freq (95% CI)	**1/50† (1/30-1/100)**	
	p Value	0.07	

p values > 0.05 indicate the data are consistent with a single-hit Poisson model.
† Rough MaSC frequency estimate (see Statistical Analyses under Methods for detail).
N.D.= not determined.

Supplemental Experimental Procedures

Mice and embryos
Actin-eGFP mice (with C57BL/6 and CD-1 mixed background) were bred and maintained in the Salk Institute animal facility according to institutional guidelines. CD-1 nulliparous and pregnant mice and CB17-SCID recipient female mice were purchased from Charles River. Timed pregnancies were setup by crossing either homozygous or heterozygous adult actin-eGFP mice with adult CD-1 mice. The morning on the day a plug was found was designated as E0.5 and the plugged female was individually housed upon discovery of the plug. At the beginning of each experiment, embryos were staged according to morphological criteria to confirm gestation period. All experiments were approved by IACUC/AAALAC.

Intact mammary gland isolation
Aseptic technique was used during adult and fetal mammary gland dissections for cell preparations. Stereoscopes (Leica) with oblique bottom illumination were used to visualize fetal mammary glands during dissection (Figure S1A). The isolated intact fetal mammary rudiments include both the epithelium and their surrounding stroma. Fetal and adult mammary glands intended for enzymatic digestions were placed directly in Epicult-B media containing collagenase and hyauronidase (see Cell preparation). Intact fetal (Figure S1A) and adult mammary fragments (~1mm in size) dissected for transplants were placed in DMEM (Mediatech) supplemented with 10% fetal bovine serum (FBS) (Chemicon). A fluorescent stereoscope (Leica) was utilized to visualize Actin-eGFP$^+$ mammary glands and Actin-eGFP$^+$ positive mammary repopulated fat pads.

Cell preparation
Adult mammary glands were obtained from 12-16-week-old nulliparous Actin-eGFP or CD-1 female mice. Minced adult mammary glands were digested for 8-12 hours at 37^{o}C in EpiCult-B media containing B supplement, collagenase and hyaluronidase. All reagents were purchased from Stem Cell Technologies (SCT), unless otherwise specified. Mammary organoids resulting from overnight digestion were treated with ammonium chloride solution then Trypsin followed by Dispase, with washes and resuspension after each treatment using Hank's Balanced Salt Solution (HBSS) supplemented with 2% FBS. Adult single cells were collected by passing the suspension through a 40μm nylon filter (BD Biosciences). *CD-1 or Actin-eGFP fetal mammary glands* were obtained from various embryonic stages. On average 150 mammary rudiments were dissected on each experimental day. Dissected fetal mammary glands were digested for 90 minutes at 37^{o}C in EpiCult-B media containing B supplement, collagenase and hyaluronidase. Fetal mammary glands were treated with Dispase, washed and resuspended with Hank's Balanced Salt Solution supplemented with 2% FBS. The collection of ~150 E13.5-E15.5 rudiments generally yielded >200,000 bulk mammary cells, which were then used for subsequent flow cytometric analyses and/or transplant studies (see below).

Cell labeling, flow cytometry and sorting
Single cell suspensions were incubated on ice with Fc receptor antibody (2.4G, SCT) for 15 minutes, then incubated with biotinylated CD31 (SCT), biotinylated CD45 (SCT) and biotinylated TER119 (SCT) for 10 minutes, and then followed by streptavidin-PerCPcy5.5 (BD Biosciences), CD24-PE (M1/69, SCT) and CD49f-FITC (GoH3, SCT) for 20 minutes. Antibody-labeled cells were resuspended and incubated in HBSS with 2% FBS containing DAPI (Roche) for live/dead discrimination. In cases where the cells came from Actin-eGFP+ donor female mice, CD49f-FITC was replaced with biotinylated CD49f (GoH3 BD Biosciences) and streptavidin-APCCy7 (BD Biosciences). In that situation, cells were incubated with biotinylated CD31, biotinylated CD45 and biotinylated TER119, followed by streptavidin-PerCPcy5.5 and washed twice before adding biotinylated CD49f and streptavidin-APCcy7 sequentially. Mammary cells were lineage depleted by gating out PerCPCy5.5 positive cells. Cell sorting was carried out on FACSDiVa cell sorter (Becton Dickinson) and the purity of sorted population was routinely >95%. Data were processed using FlowJo software.

In order to directly determine how fetal populations correspond to existing MaSC sorting strategies, we processed fetal and adult cells together. The fetal cells were isolated from eGFP positive embryos and mixed with adult non-eGFP expressing tissue for processing, labeling, and flow cytometry.

***In vivo* mammary transplantation and analysis**
The surgical technique to clear the mammary fat pads and to conduct mammary transplantation has been well established (Deome et al., 1959). Briefly, the inguinal #4 and #9 mammary glands of 21-26 day old CB17-SCID recipients were surgically removed and the cleared (epithelial-free) mammary fat pads left behind served as the transplantation sites. *Mammary transplantation of single cell suspensions*: cells (freshly dissociated and, where indicated sorted) in 2-5ul of Hank's balanced salt solution supplemented with 2% FBS, mixed with Matrigel 1:1 (BD Biosciences) and 0.05% Trypan blue (Sigma), were injected into each cleared fat pads by mouth pipette using fire polished glass capillaries (Fisher). In some

cases, the cells were not co-injected with Matrigel. *Mammary transplantation of intact mammary pieces*: a small pocket was made in the fat pad using sharp forceps (Fine Science Tool, Dumont no. 5), and then one intact mammary piece was inserted into the pocket in the fat pad. Transplanted glands were removed from the recipients 6-12 weeks post-surgery for mammary repopulation evaluation. The excised glands were laid onto slides as whole mounts and visualized for mammary regeneration either by direct fluorescence microscopy or by staining the whole mounts with carmine aluminum sulfate (Sigma). In cases where specified, some of the recipients were mated with males to evaluate alveolar development in the regenerated mammary. We scored a positive for mammary outgrowths in repopulated fat pads when at least two of the following three criteria were met; a) connected branching network, b) visible tertiary branches and c) terminal end buds.

Immunofluorescence staining and microscopic imaging

Intact mammary rudiments for whole-mount staining were prepared by dissecting and then fixing rudiments for 4 hours in 4% PFA at room temperature, washing 3 times in PBST (PBS-/0.2% Triton X-100), and then blocking and permeablizing in 10% goat serum, 0.1% Triton X-100 for 1 hour. Whole rudiments were then incubated in primary antibody overnight at 4^{o}C, washed in PBST, incubated for 1 hour in secondary antibodies, washed in PBST, and then mounted in Vectashield. Paraffin embedded sections were made by fixing mammary tissues in 4% PFA overnight, then dehydrating the tissues through 70%, 95%, and 100% ethanol, treated with xylene, washed in paraffin 5 times, and then incubated in paraffin overnight. 10-20μm sections were generated and then de-paraffinized and hydrated before retrieving antigens in citrate buffer by microwaving for 6 minutes on high power. The sections were then washed in PBS and rinsed in water. Sections were blocked for 3 hours in 10% goat serum, incubated in primary antibody overnight at 4^{o}C, incubated in secondary antibodies for 1 hour at room temperature, and then mounted in Vectashield. For staining of dissociated cells, cells were cytospun at 600 - 800RPM onto Superfrost/Plus slides (Fisher), allowed to air dry, rinsed in PBS+, and then fixed for 15min in 4% PFA (Electron Microscopy Sciences), blocked for 1 hour in 10% goat serum/PBS- at room temperature, and then incubated in primary antibodies overnight at 4^{o}C. Cytospins were then washed and incubated in secondary antibodies for 1 hour at room temperature, washed and mounted in Prolong Gold. Cytospun cells were quantified for their different subtypes using OpenLab 3.1.7 software to create density slices and run Boolean operations to count DAPI positive cells with or without different marker expression. Antibodies used were Keratin 14 (AF-64, Covance, 1:1000), Keratin 8 (Troma-1, DSHB, 1:100), CD24 (M1/69, BD Biosciences, 1:1000), CD49f (GoH3, BD Biosciences, 1:1000), Casein (a gift from Gilbert Smith and Daniel Medina, 1:25), Vimentin (AB5733, Chemicon, 1:1000) and ErbB2 (29D8, Cell Signaling, 1:500). Secondary antibodies were purchased from Molecular Probes/Invitrogen: anti-rat Alexafluor 488 (1:1000), anti-rabbit Alexafluor 568 and 660 (1:1000), anti-chicken Alexafluor 488 (1:1000). All sections were imaged using a Leica TCS SP2 AOBS confocal microscope or a Zeiss LSM 710 Laser Scanning confocal microscope.

***In vitro* three-dimensional primary, secondary and tertiary sphere forming cultures for fetal mammary cells**

All reagents were purchased from SCT except where indicated. *Suspension mammosphere culture:* freshly sorted cells were plated on ultra-low adherence plates (Corning) at a density of 1000 cells/cm^2 in Epicult-B mouse media containing B supplement, rhEGF, rhbFGF, Heparin and Penicillin/Streptomycin (Chemicon). Similar culturing conditions replacing B supplemented Epicult-B basal media with DMEM/F12 media (Cellgro) and B27 (Invitrogen) yielded similar results. *2% Matrigel culture:* freshly sorted cells or sphere derived cell suspensions were plated on ultra-low adherence plates (Corning) at a density of 1000cells/cm^2 in mammosphere media containing 2% Matrigel (growth factor reduced, BD Biosciences). Similar culturing conditions without B supplement yielded similar results. *Serial passage of spheres:* Primary spheres grown in 2% Matrigel were isolated by incubating for 1hr on ice in Cell Recovery Solution (BD Biosciences), were treated with Trypsin (0.05%) for 5min at 37ºC, washed, and then treated with dispase at room temperature for 5-10min. Single cells were collected by passing cell suspension through a 30μm filter prior to plating on ultra-low adherence plates (Corning) at a density of 1000 cells/cm^2 in 2% Matrigel media. *100% Matrigel culture:* freshly sorted cells were seeded on top of ~30μl bed of Matrigel (growth factor reduced) per well of an 8-well chamber slide (BD Falcon 354108) in 2% Matrigel media. Vehicle (DMSO), Lapatinib (LC Laboratories), Neratinib (HKI-272, Pfizer) or FGFR inhibitor (PD173074, gift from the Verma lab, Salk Institute) were added at the indicated doses to the media. Media was changed every 3 days. After 7-10 days, cultures were photographed and spheres were scored. *Clonal sphere culture.* Two different cell plating strategies were employed to demonstrate that the fMaSC population derived spheres originated from single cells rather than from aggregates. First, single cells were sorted into 96 well plates at a single cell per well density. The cells were cultured in Epicult-B mouse media supplemented with 2% Matrigel (growth factor reduced), B supplement, rhEGF, rhbFGF, Heparin and Penicillin/Streptomycin. New media was added every 3 days. After 7-10 days, cultures were photographed and spheres were scored (Figure 2B and S2A). In parallel, we also isolated the fMaSC from wild-type CD1 and Actin-eGFP, mixed the cells in either 1:1 or 1:4 ratio, and seeded at low density on top of Matrigel (growth factor reduced). The cells were cultured in 2% Matrigel media. New media was added every 3 days. After 8-10 days, cultures were photographed and spheres were scored. All of the spheres from the fMaSC population that were examined were either eGFP+ or non eGFP with the exception of one

sphere (out of 208), which consisted of a mixture of eGFP+ and eGFP- cells (Figure 2B, S2B and S2C). The fSTR population from $eGFP^+$ and $eGFP^-$ mice were cultured as described above, but in suspension on ultra-low adherent plates and in mammosphere media in the absence of B supplement at both low and high densities.

Two-dimensional control cultures
10,000 MCF10A/HER2 cells (Wang et al., 2006) or BT549 (ATCC) cells were plated in triplicate wells of a 96 well dish in RPMI supplemented with 10% FBS and insulin. MCF10A/HER2 cells were additionally supplemented with 5% horse serum, rhEGF, hydrocortisone, cholera toxin, insulin and Penicillin/Streptomycin (Chemicon). Cells were allowed to adhere and recover for 24 hours. Cells were then treated with Lapatinib or Neratinib at the indicated doses diluted in DMSO or with Vehicle (DMSO) alone for 48 hours and live cells were counted using trypan blue exclusion.

Quantitative real-time PCR analyses on Estrogen Receptor, Progesterone Receptor, and ErbB family members
RNA was isolated, reverse transcribed, and pre-amplified from 40,000 cells using the CellsDirect kit from Invitrogen. Pre-amplification and QPCR was performed using TaqMan® Gene Expression Assays (Applied Biosystems, see below). The realtime PCR was carried out according to the manufacturer's recommendations on an ABI 7900HT Fast Real-Time PCR system. Data was analyzed using Applied Biosystems Signal Detection System 2.3 and Microsoft Excel. Cycle thresholds (Ct) were normalized between samples using the HPRT gene. Relative fold differences between means was calculated using the formula $2^{\Delta CT}$.

Single Cell qRT-PCR analysis
For single cell gene expression analyses, we used qPCR 96.96 dynamic arrays (Fluidigm). Single cells were sorted by FACS into a total of four 96-well plates containing a reaction mix for reverse transcription (CellsDirect, Invitrogen) and pre-amplification (0.2X concentration of Taqman Assays, Applied Biosystems, see below for list). In addition, 10, 100 and 1000 cells were sorted in triplicate. The cDNA samples were amplified for 18 PCR cycles and then diluted five fold in TE. All samples were evaluated for expression of GAPDH on an ABI 7900HT. The 10, 100, and 1000 cell dilutions were used to create a standard curve such that the expected Ct value for a single cell could be extrapolated. We used single cell samples that had detectable GAPDH levels roughly equivalent to single cells. The dynamic array chip was primed using control line fluid (Fluidigm) in a HX IFC controller (Fluidigm) and then 2.25μL of the cDNA samples were transferred into the chip sample inlets after mixing with Taqman universal PCR master mix (2.5μL, Applied Biosystems) and sample loading reagent (0.25μL, Fluidigm). The individual Taqman assays (Applied Biosystems) were mixed with equal volumes of assay loading reagent (Fluidigm) and then transferred into the chip assay inlets. The chip was then loaded by the chip loader and then transferred to the reader (Biomark, Fluidigm) for thermocycling and fluorescent quantification.

The fMaSC population was analyzed by running duplicate chips. All sample Ct values were normalized to GAPDH, cells with no detectable GAPDH expression were dropped from analysis. GAPDH normalization included a 10 – 20 fold expression correction to visualize relative expression within positive ranges. HPRT and/or GusB were also included as housekeeping genes, and normalization to these genes gave similar results but reduced the number of processed samples. ΔCt values were subjected to log2 redistribution and then clustered using the Pearson correlation coefficient.

Statistical Analysis
Limiting dilution analysis of mammary repopulating unit frequency was performed using the ELDA web interface (http://bioinf.wehi.edu.au/software/elda/index.html) (Hu and Smyth, 2009), which includes a goodness of fit test based on the complementary loglog (cloglog) model originally developed by Bonnefoix and colleagues (Bonnefoix et al., 1996). ELDA was developed to account for limiting dilution analysis data where the assays are predominantly all positive or all negative. The active cell frequency estimate is based on the single-hit Poisson model, with frequency range given by the usual two sided 95% Wald confidence intervals except in cases with 0% or 100% responses where a modified Clopper-Pearson 1-sided confidence interval was given (Hu and Smyth, 2009). In instances where the single-hit Poisson model hypothesis could not be assessed because the cloglog model did not hold, a situation which can result from insufficient number of repopulated fat pads, those frequencies (†) are noted as "rough MaSC frequency estimate" (as recommended in personal communication by Thierry Bonnefoix at Institut National de la Sante de la Recherche Medicale, INSERM U823, Institut Bonniot, Grenoble, France).

Microarray Analyses and Statistics
To obtain sufficient material for RT-PCR and microarray analysis on rare biological samples (E15.5, fMaSC (E18.5, $CD24^{high}CD49f^{high}$) and fSTR (E18.5 $CD24^{med/low/neg}$)), independent replicate pools were created. Each pool consisted of RNA

isolated and amplified from at least two independent dissection sessions. For each E18.5 dissection session, we isolated as much material as possible from embryos between 5:00AM and 8:00AM on the day of dissociation and sorting. This generally consisted of between 100 and 200 rudiments from 10-20 female embryos derived from 2-4 timed pregnant female mice and yielded up to 30,000 fMaSC cells. The E15.5 array data was derived from a single dissection session per sample to obtain at least 100 E15.5 mammary buds per sample. Adult samples were derived from a single dissection session each using 4 adult inguinal (#4) mammary glands from two mice as the starting material. Dissociated unsorted cells were gently centrifuged and resuspended in cold lysis buffer, and total RNA was extracted using the RNAqueous kit (Ambion). For sorted cells, we sorted directly into ice cold lysis buffer. RNA integrity was analyzed using an Agilent 2100 Bioanalyzer and RNA quality measures (RIN scores) were greater than 9.0 when sufficient RNA to yield a reading was present. DNase treated RNA samples were subsequently reverse transcribed using Superscript III reverse transcriptase (Invitrogen) and a custom T7 oligo-dT primer, 5'-GGCACGTGAATTGTAATACGACTCACTATAGGGAGGCGG$(T)_{20}$-3' (pre-amplification) or random hexamers (post-amplification). Samples were amplified according to the linear procedure described by Van Gelder et. al. (Van Gelder et al., 1990) using T7 RNA Polymerase (Ambion) and a 14 hour IVT incubation time. Yield was determined using a NanoDrop ND8000 small scale spectrophotometer (Thermo Scientific).

Complimentary DNA libraries were combined into independent replicate pools as described above and were labeled using the Nimblegen One-Color DNA Labeling Kit, hybridized to a Nimblegen 12x135k MM9 mouse microarray (Roche Nimblegen), scanned on a Genepix4000B, all according to manufacturer's recommendations and raw intensities were RMA normalized (Irizarry et al., 2003) at the UCSD-GeneChip Microarray Core. The MIAME compliant array data are available from the gene expression omnibus at http://www.ncbi.nlm.nih.gov/ under accession GSE27027.

We removed probes with max intensity for any sample lower than the 10^{th} percentile of mean probewise intensities from further analysis to reduce noise. This minor noise reduction corresponds roughly to the minimum intensity yielding fold differences of >2-fold between any sample type mean and the overall mean across all samples. Intensities were Log2 transformed and median centered for each probe. Differentially expressed genes were subsequently identified using the Significance Analysis of Microarrays (SAM) (Tusher et al., 2001) plugin for Microsoft Excel in pairwise comparisons between fMaSC (E18.5 $CD24^{high}CD49f^{high}$), fSTR (E18.5 $CD24^{low\text{-}med}$) and adult MaSC (aMaSC; $Lin^{-}CD24^{med}CD49f^{high}$) (Stingl et al., 2006) samples with FDR manually adjusted to <10%. The fold difference limit was set at 1.5 fold, however the minimum fold difference identified under these criteria for any sample was 2.3 fold. The mean and median fold differences across all samples were 7.6 fold and 4.7 fold respectively. SAM results including individual fold differences are listed in Table S4. These analyses resulted in the identification of 1,308 probes upregulated in the fMaSC population relative to fSTR population and 1,047 probes downregulated in the fMaSC population relative to the fSTR population (Table S4 and Figure 3A). The 1,047 probes can conversely be regarded as upregulated in the fSTR relative to fMaSC population and were therefore designated as the fSTR signature.

The fMaSC/fSTR reciprocal interaction model (Figure 5) was adapted from GeneGo interaction networks (http://genego.com) and was constructed using fMaSC and fSTR gene sets with automated filters for "receptors and ligands" and manual filtering for direct interactions. GeneGo uses a currated interaction database to designate input genes having gene products that are thought or known to interact. We manually filtered the results to leave only those input genes exhibiting at least one interaction to another input gene. As such, the model presents a restricted set of candidate interactions.

Molecular Function, Biological Process and Pathway enrichment analyses were carried out using the BINGO plug-in for Cytoscape (Cline et al., 2007; Maere et al., 2005) or Gene Ontology and KEGG Pathway annotations in GeneGo and through the DAVID website (http://david.abcc.ncifcrf.gov/) with the background created using the full list of probes on the Nimblegen array. The annotations we report have $p<0.01$ for BINGO, and for DAVID, met the modified Fisher Exact P-Value, EASE criteria of $p<0.05$ for whole gene set enrichment and $p<0.1$ for small gene clusters. Small clusters (Figure 6E and Table S6) utilized the whole database as background. Translation of probe IDs into Entrez IDs and human orthologues was carried out using the Clone Gene ID converter at CNIO (http://idconverter.bioinfo.cnio.es/IDconverter.php) followed by the Ensembl database at Biomart (http://biomart.org) and finally DAVID (http://david.abcc.ncifcrf.gov) to fill in additional IDs not found by CNIO. All resources were based on NCBIM37 and GRCh37.p2 genome builds. These "translated" ID's were subsequently mapped for human orthologues using the human mouse orthology list downloaded from the Jackson laboratory website on September 4, 2011, (http://jax.org). The step-wise, translated gene lists are given in Table S4 and S5 along with the number of extant probes at each stage. Reduction in gene number during translation is a well-known phenomenon, since not all probes on the microarray correspond to known, unique genes. Therefore the number of genes identified as differentially expressed by microarray will be fewer than the number of differentially expressed probes identified. Similarly, not all mouse genes have known human orthologues. Therefore the number of genes translated into

human orthologues will be fewer than the starting number of genes. Finally, not all orthologous human genes will be represented on human microarrays leading to a further reduction in genes tested for differential expression in human tumor microarrays.

QRT-PCR was performed on select targets for orthongonal confirmation of differential expression (Figure S4) using TaqMan® Gene Expression Assays (Applied Biosystems, see Taqman assay table). PCRs on material amplified as described above were carried out according to the manufacturer's recommendations on an ABI 7900HT Fast Real-Time PCR system. Data was analyzed using Applied Biosystems Signal Detection System 2.3 and Microsoft Excel. Ct's were set manually to a consensus phase of exponential amplification for the entire population and samples showing erratic, grossly non-exponential or non-monophasic amplification were excluded. Ct's were normalized between samples using the HPRT gene. Relative fold differences between means were calculated using the idealized formula $2^{\Delta CT}$ and the value for the cell type with the higher mean Ct for each gene was set to one for Figure S4B. *p* values were determined by Students t-test (two-tailed, equal variance).

Signatures from published work representing differentially expressed adult mMaSC, mLuminal progenitor, mMature luminal and mStromal genesets were generated from normalized, Log2 transformed array data associated with Lim et al. (Lim et al., 2010) downloaded from the gene expression omnibus at http://www.ncbi.nlm.nih.gov/ (GSE19446) and were analyzed using SAM with median centering and FDR manually set to <0.1 as described above to generate population specific gene sets since the complete list of individual genes comprising the reported signatures were not publicly available at the time of these analyses. The hMaSC, hLuminal progenitor, hMature luminal and hStromal signatures were as reported in Lim et al. (Lim et al., 2009). We also determined that 95% of the differentially expressed genes reported using LIMMA at FDR=0.05 (from the original report) were identified as differentially expressed using SAM at FDR<0.1 on the primary array data downloaded from GEO (GSE16997) (not shown). The E12.5 mammary epithelial and mammary mesenchyme signatures were from Wansbury et al. (Wansbury et al., 2011). The "cultured hMaSC" geneset reported in Pece et al. (Pece et al., 2010) was taken directly from the published report.

Gene set similarities (Figure S5) were determined by enumerating the overlap in the gene lists resulting from SAM analyses or as published in original reports (Lim et al., 2009; Pece et al., 2010). A cumulative hypergeometric probability was calculated for the overlap based on 20,309 and 19,828 probes in compendiated mouse and human arrays identified below, respectively. Probabilities calculated for signature overlaps in Figure 6B used the 3338 genes represented in at least one signature as the set of possible genes.

To assess fetal gene expression profile enrichment in tumor samples, we obtained two independent published, annotated microarray compendia from the public domain (Ben-Porath et al., 2008; Prat et al., 2010). Human tumor data was downloaded as annotated, pre-normalized and centered values from Ben-Porath et al. (http://jura.wi.mit.edu/bioc/benporath/) and represents ~1,200 tumor samples from 6 independent studies (Ben-Porath et al., 2008) or alternatively from Prat et al. 2010 comprising 295 samples. Intrinsic subtype annotations were as determined in Ben-Porath et al. (Ben-Porath et al., 2008) except that a subset of tumors in the Ben-Porath compendium were re-annotated as "Claudin low-like" and "Metaplastic-like" based on their repression or enrichment for gene clusters and signatures described in Hershkowitz et al. (Herschkowitz et al., 2007) and Hennesey et al. (Hennessy et al., 2009) as detailed in supplemental Table S7. These enrichments as well as the gene set enrichments among tumor samples we observed in Figure 6A were determined according to previously published methods (Segal et al., 2005) using Genomica software (http://genomica.weizmann.ac.il/). Briefly, genes expressed at least two fold above or below the compendium mean were considered differentially expressed. We then assessed the fraction of over- or underexpressed genes that belong to each tested gene set, calculating a *P* value according to the hypergeometric distribution. This was repeated for every sample, using a threshold of $P < 0.05$ for significant enrichment. Benjamini-Hochberg multiple hypothesis testing correction was employed with FDR <0.05. Random gene sets equivalent in size to population derived gene sets were constructed from random ranking of genes using the Excel random number generator. Five or more random gene sets were generated for each population derived gene set and never resulted in class-wise enrichments comparable to population derived gene sets. One example is shown in Figure 6A. The same procedure was carried out independently on array data comprising the NKI295 (Parker et al., 2009) and UNC datasets (Prat et al., 2010) obtained from the UNC microarray database at https://genome.unc.edu/.

To compare enrichment patterns for different intrinsic subtype or grade designations (Figure 6C), we calculated the fraction of samples of a given designation showing significant enrichment or repression for a particular gene set, and assigned a *P* value according to the hypergeometric distribution. In other experiments, we established that there exists general agreement

between this enrichment approach (Segal et al., 2005) and an alternative statistical strategy, GSEA, (Subramanian et al., 2005) in subtype gene set enrichments (not shown).

The 96 genes in each fetal gene set with the greatest variance across the breast cancer arrays were subsequently selected for sample-class and gene-cluster discovery. We chose 96 high variance genes since higher variance can yield greater statistical power in delineating gene and sample classes and in order to facilitate ongoing studies and potential clinical applications in standard 12 by 8 formats. To select coordinately expressed gene subsets, we took a clustering approach similar to that originally used to identify 'intrinsic' breast cancer subtypes, although care must be taken in interpreting hierarchical clusters here as in the original studies (Perou et al., 1999) since these can be subject to initial condition effects and the specific gene set employed. Clustering and graphic representations were generated in the TM4 suite MeV software (Saeed et al., 2003). Hierarchical clustering used euclidean distance and average linkage as metrics. Nine clusters of 5 or more genes per cluster were selected for further characterization following assessment of the stability of their coordinate expression by measuring their reproducibility under permutation analysis using the Support Trees algorithm in MeV (Figure S6D).

Kaplan-Meier analysis was carried out on the NKI-295 data set (van de Vijver et al., 2002) as annotated in Parker et al. (Parker et al., 2009) using MedCalc™. *P* values represent log rank test results and scores can be corrected for multiple testing of 9 gene clusters by the formula, P_{shown}x9=$P_{corrected}$. Multivariate analysis also used Medcalc and the Parker-annotated, NKI-295 dataset. Significant enrichment or depletion for individual subsignatures was determined as above and tumor subsignature annotations were tested in models containing various combinations of categorical lymph node positivity, tumor size, ER status and Grade as indicated.

Taqman Assays Utilized

Gene	Assay ID	Gene	Assay ID	Gene	Assay ID
Abcg2	Mm00496364_m1	Fgf10	Mm00433275_m1	Ngfr	Mm01309635_m1
Arhgap5	Mm00501557_m1	FZD9	Mm01206511_s1	Nr2f1	Mm00657937_m1
Axin2	Mm00443610_m1	GAPDH	Mm99999915_g1	Nrg1	Mm01212130_m1
Bmi1	Mm00776122_gH	gata3	Mm00484683_m1	Nrg2	Mm01158088_m1
CD10 (Mme)	Mm01285052_m1	Gli3	Mm00492333_m1	NTRK3	Mm00456222_m1
CD24a	Mm0078258_sH	Gnaq	Mm00492381_m1	Olfr620	Mm00748427_s1
Cd24a	Mm00782538_sH	Gnas	Mm00507037_m1	p63	Mm00495788_m1
Cd34	Mm00519283_m1	GusB	Mm03003537_s1	PDGFc	Mm00480205_m1
Cd44	Mm01277163_m1	HPRT	Mm01324427_m1	PDGFra	Mm01211694_m1
Cdkn1a	Mm00432448_m1	Hprt1	Mm01545399_m1	Pgr	Mm00435628_m1
Cldn6	Mm00490040_s1	Itga4	Mm00439770_m1	Pkm2	Mm00834102_gH
Cldn9	Mm00517434_s1	Itga6	Mm00434375_m1	Plp1	Mm01297210_m1
Cmtm5	Mm00509113_m1	Itgb1	Mm01253227_m1	Reln	Mm00465200_m1
Cnp	Mm01306640_m1	K05	Mm00503549_m1	RunX1	Mm01213405_m1
Cxcr4	Mm01292123_m1	K08	Mm00835759_m1	Sema3b	Mm00436477_m1
Cyclin D1	Mm00432360_m1	K14	Mm00516876_m1	Serpinb5	Mm00436763_m1
Ddr1	Mm01273494_g1	K18	Mm01601702_g1	Sfrp1	Mm00489161_m1
Dkk1	Mm00438422_m1	K19	Mm00492980_m1	Snai2	Mm00441531_m1
EDNRB	Mm00432989_m1	L1cam	Mm00493049_m1	Sox10	Mm01300162_m1
EGFR	Mm0043023_m1	Lef1	Mm00550265_m1	Sox2	Mm00488369_s1
EGFR	Mm0043023_m1	Lgr5	Mm00438890_m1	Tbx3	Mm00809779_s1
EpCam (Tacstd1)	Mm00493214_m1	Lmo4	Mm00495373_m1	Tcf3	Mm00493456_m1
Erbb2	Mm00658541_m1	Ly6a	Mm00726565_s1	Tnc	Mm00495662_m1
Erbb3	Mm01159990_g1	Mag	Mm00487538_m1	Tlr3	Mm01207403_m1
Erbb4	Mm01256793_m1	Msi2	Mm00475180_m1	Tspan8	Mm00524563_m1
Esr1	Mm01191130_m1	Muc1	Mm00449604_m1	Twist1	Mm00442036_m1
Esr1	Mm00433149_m1	Myc	Mm00487803_m1	Vim	Mm00449208_m1
Fgf07	Mm00433291_m1	Ncam1	Mm03053534_s1		

Supplemental References

Ben-Porath, I., Thomson, M. W., Carey, V. J., Ge, R., Bell, G. W., Regev, A., and Weinberg, R. A. (2008). An embryonic stem cell-like gene expression signature in poorly differentiated aggressive human tumors. Nat Genet *40*, 499-507.

Bonnefoix, T., Bonnefoix, P., Verdiel, P., and Sotto, J. J. (1996). Fitting limiting dilution experiments with generalized linear models results in a test of the single-hit Poisson assumption. J Immunol Methods *194*, 113-119.

Cline, M. S., Smoot, M., Cerami, E., Kuchinsky, A., Landys, N., Workman, C., Christmas, R., Avila-Campilo, I., Creech, M., Gross, B., *et al.* (2007). Integration of biological networks and gene expression data using Cytoscape. Nat Protoc *2*, 2366-2382.

Deome, K. B., Faulkin, L. J., Jr., Bern, H. A., and Blair, P. B. (1959). Development of mammary tumors from hyperplastic alveolar nodules transplanted into gland-free mammary fat pads of female C3H mice. Cancer Res *19*, 515-520.

Hennessy, B. T., Gonzalez-Angulo, A. M., Stemke-Hale, K., Gilcrease, M. Z., Krishnamurthy, S., Lee, J. S., Fridlyand, J., Sahin, A., Agarwal, R., Joy, C., *et al.* (2009). Characterization of a naturally occurring breast cancer subset enriched in epithelial-to-mesenchymal transition and stem cell characteristics. Cancer Res *69*, 4116-4124.

Herschkowitz, J. I., Simin, K., Weigman, V. J., Mikaelian, I., Usary, J., Hu, Z., Rasmussen, K. E., Jones, L. P., Assefnia, S., Chandrasekharan, S., *et al.* (2007). Identification of conserved gene expression features between murine mammary carcinoma models and human breast tumors. Genome Biol *8*, R76.

Hu, Y., and Smyth, G. K. (2009). ELDA: extreme limiting dilution analysis for comparing depleted and enriched populations in stem cell and other assays. J Immunol Methods *347*, 70-78.

Irizarry, R. A., Bolstad, B. M., Collin, F., Cope, L. M., Hobbs, B., and Speed, T. P. (2003). Summaries of Affymetrix GeneChip probe level data. Nucleic Acids Res *31*, e15.

Lim, E., Vaillant, F., Wu, D., Forrest, N. C., Pal, B., Hart, A. H., Asselin-Labat, M. L., Gyorki, D. E., Ward, T., Partanen, A., *et al.* (2009). Aberrant luminal progenitors as the candidate target population for basal tumor development in BRCA1 mutation carriers. Nat Med *15*, 907-913.

Lim, E., Wu, D., Pal, B., Bouras, T., Asselin-Labat, M. L., Vaillant, F., Yagita, H., Lindeman, G. J., Smyth, G. K., and Visvader, J. E. (2010). Transcriptome analyses of mouse and human mammary cell subpopulations reveal multiple conserved genes and pathways. Breast Cancer Res *12*, R21.

Maere, S., Heymans, K., and Kuiper, M. (2005). BiNGO: a Cytoscape plugin to assess overrepresentation of gene ontology categories in biological networks. Bioinformatics *21*, 3448-3449.

Parker, J. S., Mullins, M., Cheang, M. C., Leung, S., Voduc, D., Vickery, T., Davies, S., Fauron, C., He, X., Hu, Z., *et al.* (2009). Supervised risk predictor of breast cancer based on intrinsic subtypes. J Clin Oncol *27*, 1160-1167.

Pece, S., Tosoni, D., Confalonieri, S., Mazzarol, G., Vecchi, M., Ronzoni, S., Bernard, L., Viale, G., Pelicci, P. G., and Di Fiore, P. P. (2010). Biological and molecular heterogeneity of breast cancers correlates with their cancer stem cell content. Cell *140*, 62-73.

Perou, C. M., Jeffrey, S. S., van de Rijn, M., Rees, C. A., Eisen, M. B., Ross, D. T., Pergamenschikov, A., Williams, C. F., Zhu, S. X., Lee, J. C., *et al.* (1999). Distinctive gene expression patterns in human mammary epithelial cells and breast cancers. Proc Natl Acad Sci U S A *96*, 9212-9217.

Prat, A., Parker, J. S., Karginova, O., Fan, C., Livasy, C., Herschkowitz, J. I., He, X., and Perou, C. M. (2010). Phenotypic and molecular characterization of the claudin-low intrinsic subtype of breast cancer. Breast Cancer Res *12*, R68.

Saeed, A. I., Sharov, V., White, J., Li, J., Liang, W., Bhagabati, N., Braisted, J., Klapa, M., Currier, T., Thiagarajan, M., *et al.* (2003). TM4: a free, open-source system for microarray data management and analysis. Biotechniques *34*, 374-378.

Segal, E., Pe'er, D., Regev, A., Koller, D., and Friedman, N. (2005). Learning Module Networks. The Journal of Machine Learning Research *6*, 557-588.

Stingl, J., Eirew, P., Ricketson, I., Shackleton, M., Vaillant, F., Choi, D., Li, H. I., and Eaves, C. J. (2006). Purification and unique properties of mammary epithelial stem cells. Nature *439*, 993-997.

Subramanian, A., Tamayo, P., Mootha, V. K., Mukherjee, S., Ebert, B. L., Gillette, M. A., Paulovich, A., Pomeroy, S. L., Golub, T. R., Lander, E. S., and Mesirov, J. P. (2005). Gene set enrichment analysis: a knowledge-based approach for interpreting genome-wide expression profiles. Proc Natl Acad Sci U S A *102*, 15545-15550.

Tusher, V. G., Tibshirani, R., and Chu, G. (2001). Significance analysis of microarrays applied to the ionizing radiation response. Proc Natl Acad Sci U S A *98*, 5116-5121.

van de Vijver, M. J., He, Y. D., van't Veer, L. J., Dai, H., Hart, A. A., Voskuil, D. W., Schreiber, G. J., Peterse, J. L., Roberts, C., Marton, M. J., *et al.* (2002). A gene-expression signature as a predictor of survival in breast cancer. N Engl J Med *347*, 1999-2009.

Van Gelder, R. N., von Zastrow, M. E., Yool, A., Dement, W. C., Barchas, J. D., and Eberwine, J. H. (1990). Amplified RNA synthesized from limited quantities of heterogeneous cDNA. Proc Natl Acad Sci U S A *87*, 1663-1667.

Wang, X., Kua, H. Y., Hu, Y., Guo, K., Zeng, Q., Wu, Q., Ng, H. H., Karsenty, G., de Crombrugghe, B., Yeh, J., and Li, B. (2006). p53 functions as a negative regulator of osteoblastogenesis, osteoblast-dependent osteoclastogenesis, and bone remodeling. J Cell Biol *172*, 115-125.

Wansbury, O., Mackay, A., Kogata, N., Mitsopoulos, C., Kendrick, H., Davidson, K., Ruhrberg, C., Reis-Filho, J. S., Smalley, M. J., Zvelebil, M., and Howard, B. A. (2011). Transcriptome analysis of embryonic mammary cells reveals insights into mammary lineage establishment. Breast Cancer Res *13*, R79.